Université Abou Moumouni

Doctoral Research Program on Climate Change and Energy

(DRP-CCE)

NIGER

INTERNATIONAL MASTER PROGRAM

IN RENEWABLE ENERGY AND GREEN HYDROGEN

SPECIALITY: PHOTOVOLTAICS FOR GREEN HYDROGEN TECHNOLOGY

MASTER THESIS

Topic:

DEVELOPMENT OF A SETUP FOR ELECTROLUMINESCENCE MEASUREMENT

PRESENTED THE 28/09/2023 AND BY:

GEORGETTE CELESTINE UDO

M. Amadou SEIDOU MAIGA	Président	Professeur Titulaire, Laboratoire d'Electronique, Informatique, Télécommunication et Energies Renouvelables, UFR des Sciences Appliquées et des technologies, Université Gaston Berger, Saint-Louis (Sénégal)
M. Moctar MOSSI	Examinator	Maitre-Assistant, Département de Physique, Faculté des Sciences et Technique, Université Abdou Moumouni (Niger)
M. Rabani ADAMOU	Local Supervisor	Professeur Titulaire, Département de Chimie, Faculté des Sciences et Technique, Université Abdou Moumouni (Niger)
M. Abdoulkadri AYOUBA MAHAMANE	Local Co-supervisor	Maitre de Assistant, Département de Chimie, Faculté des Sciences et Technique, Université Abdou Moumouni (Niger)
M. Jurgen H. WERNER	Co-supervisor in German	Professor of Institut für Photovoltaik Uni Stuttgart, (Germany)
M. Uwe RAU	Supervisor in German	Full professor at RWTH Aachen - Faculty Electrical Engineering and Computer Science, chair of photovoltaics (Germany)

Academic year 2022-2023

DEDICATION

I dedicate this thesis to my mother, whose love, prayers, and support helped me get through this, as well as to my supervisors' commitment and encouragement.

ACKNOWLEDGEMENT

I thank God for the successful completion of my master's thesis.

I would like to thank the German Ministry of Education and Research BMBF and the West African Science Service Centre for Climate Change and Adaptable Land Use (WASCAL) for this scholarship. I also would like to express my gratitude to my host university Abdou Moumuni University for their tutelage and knowledge impacted which aided me in getting this master's degree.

I am grateful to Prof. Adamou Rabani (Director of WASCAL DRP CCE), Ass. Prof. Inoussa Maman Maarouhi (Coordinator and Deputy Director of Wascal DRP-CCE), Ass. Prof. Mounkaila Saley Moussa (Scientific Coordinator Wascal DRP-CCE) and Dr Ayouba Mahamane Abdoulkadri (Coordinator IMP-EGH Program, Wascal DRP-CCE) for all their efforts to the success of this program.

I owe a great deal of gratitude to Prof. Dr. Jürgen Werner, Senior Professor and former Director of the Institute for Photovoltaics, University of Stuttgart, Dr. Liviu Stoicescu, Solar Center, Stuttgart, and Prof. Dr. Uwe Rau, IEK 5, Forschungszentrum Jülich whose directions, knowledge, and constant support helped to shape my research. My sincere gratitude also goes out to my parents, whose unwavering support and sacrifices made this phase of my life possible.

I am grateful to Prof. Dr. Michael Saliba, Director of the Institute for Photovoltaics, University of Stuttgart, and staffs of the institute for providing an enabling environment for the experiments conducted in this study and assistance in accessing resources.

Finally, I want to thank my friends for supporting me through the difficulties of writing my thesis. Your encouragement and friendship were the pillars that sustained me. I really appreciate your contributions to this adventure.

TABLE OF CONTENTS

DEDICATION ii
ACKNOWLEDGEMENT iii
ABSTRACT viii
RESUME ix
INTRODUCTION 1
1. Background 1
2. Problem Statement 3
3. Research Question 3
4. Research Hypothesis 4
5. Objectives of Study 4
6. Significance of Study 4
6. Structure of The Thesis 4
CHAPTER 1: LITERATURE REVIEW 5
1.1 General aspects: 5
1.2 Electroluminescence Spectrum of Silicon 5
CHAPTER 2:MATERIALS AND METHODOLOGY 8
2.1 Electroluminescence detection setup 8
2.1.1 Utilization of a commercial camera for measurement 9
2.2 Canon EOS 4000d 10
2.2.1 Camera modifications 12
2.2.2 Filters 12
2.2.3 Transmission test 14
2.2.4 Camera Calibrations 14
2.3 Camera Settings 15
2.3.1 Shutter time t_s 15
2.3.2 F-number fN 15
2.3.3 ISO value 16
2.4 Power Supply 16
2.5 Temperature Sensor 17
2.6 Photovoltaic Modules 19
2.7 Softwares 21
2.7.1 Softwares For Brightness Measurements 21
2.7.2 Software For Data Plotting 21
2.8 Methodology 22

2.9 Processing....22
CHAPTER 3 RESULTS AND DISCUSSION....23
3.1 Preliminary results....23
3.2 Electroluminescence Measurements....29
3.2.1 Luminescence quantum efficiency EQE_{LED}....30
3.2.2 Brightness and Camera Model....30
3.2.2.1 Brightness parameters....30
3.2.2.2 Brightness parameters and exposure X....31
3.2.2.3 Saturation behavior....32
3.3.1 Reciprocity theorem....42
3.3.2 Experimental analysis....43
CONCLUSION....47
REFERENCES....48
APPENDIX....51

LIST OF FIGURES

Figure 1: a) Electroluminescence & b) Photoluminescence. (Ye et al., 2014; Yoshikawa et al., 2017) 6
Figure 2: Electroluminescence of Silicon (Ciocia et al., 2019) 7
Figure 3: Setup of the project 8
Figure 4: Real Setup of The Electroluminescence Measurement 9
Figure 5: Working Process of A CMOS Camera (Jain, 2016) 10
Figure 6 : Canon EOS 4000d Camera 11
Figure 7:Transmission Curve Filters And Sensors Channels Of A Camera (IR-Photo.Net | Infrared Photography.) 12
Figure 8: Heliopan RG850 Filter 13
Figure 9: Measured Transmission curve of the filter used. 13
Figure 10: UV VIS Spectrometer 14
Figure 11 : F-Numbers and Area of The Camera Iris (Which Aperture Is Best for Portraits or Landscape.) 16
Figure 12: Delta Elektronika Power Supply 17
Figure 13: PT100 and The Microcontroller 18
Figure 14: Measurement of El of a Cell with Image J 21
Figure 15: Raw Electroluminescence Image and Background Image of a Trina Module. 23
Figure 16: Trina Module Measured for Electroluminescence 23
Figure 17: For Low Currents Electroluminescence Increases Linearly. For Currents Above I = 4A, The Electroluminescence Deviates from Linearity and Goes into Saturation 24
Figure 18: For Long Shutter Times, The Brightness Decreases More And More From A Linear Behavior 26
Figure 19: The Saturation Behavior Is Also Observed For Increased Shutter Areas. 27
Figure 20: For Larger ISO, Saturation Is Observed. 28
Figure 21: Behavior of Separate Color Channels And Their Summation (Monochrome) 29
Figure 22: Universal Brightness Curve Depends Only on The Exposure X And Not on The Single Values of The Camera Settings. 32
Figure 23: Changes In EL Brightness as Shutter Time and F-Number Changes in The Maysun Module. 34
Figure 24: Changes In EL Brightness as Shutter Time and F-Number Changes in The Sun power module. 35
Figure 25: Changes In EL Brightness as Shutter Time and F-Number Changes In The Chinalight Module. 35
Figure 26: Changes In EL Brightness as Shutter Time and F-Number Changes in The Sun Electronics Module. 36
Figure 27: Changes In EL Brightness as Shutter Time and F-Number Changes in The Yingli Module. 36
Figure 28: EL Image showing faults & normal image of Chinalight module. 38
Figure 29: Normal IV Curve of The Chinalight Module Indicating No Faults. 39
Figure 30: Trina Plot Showing Where the Histogram Images are Taken. 39
Figure 31: Histograms Showing The EL Brightness in Pixels at Different Measurements. 40
Figure 32: To View the Difference In Electroluminescence Between Monocrystalline And Multi-crystalline Modules 41
Figure 33: The open circuit voltage follows the log of S_H. The red line is the best fit to the experimental data with a slope of 2.30 kT/q ≈ 60 mV at room temperature 43

Figure 34: External radiative quantum efficiencies of the measured solar modules. The open circuit voltage depends logarithmically on the EQE_{LED}. We assumed that all cells in the modules have the same radiative limit of the open circuit voltage. The red curve fits the data well.....46

LIST OF TABLES

Table 1: Measured Values of Trina Electroluminescence Test Showing the Temperature Changes. .. 18
Table 2: List of Panels Characteristics.....20
Table 3: Measured Values of Trina Module Electroluminescence Test 25
Table 4: Detailed characteristics of module cells.....37
Table 5: Brightness slope values and calculated radiative quantum efficiencies of our modules.....46

ABSTRACT

As technology advances cost reduction and process optimization is very important. The technology of electroluminescence is growing but it is still quite expensive especially for developing scientific laboratories that are carrying out research in photovoltaics. Electroluminescence requires a little period of time to provide a wide range of information about the photovoltaic module being measured.

The approach used in the course of this thesis is the process of using a commercial camera to carry out dark electroluminescence. The measurements carried out on different photovoltaic modules (both multicrystalline and monocrystalline) at different camera settings such as the variations of the f-number, shutter speeds and at different short circuit current and the results gotten from this were used to experimentally prove the Rau's reciprocity theorem.

It is indeed proven that solar cells/ modules with a higher open circuit voltage (Voc) has a higher electroluminescence quantum efficiency EQE. For every 60mV increase of the open circuit voltage the electroluminescence quantum efficiency increases by a factor of ten.

This project is able to give an experimental approach Rau reciprocity theorem and also creating an affordable set up for electroluminescence measurements.

Keywords: Electroluminescence quantum efficiency, reciprocity theorem, camera model, electroluminescence image brightness, and open circuit voltage.

RESUME

À mesure que la technologie progresse, la réduction des coûts et l'optimisation des processus sont très importantes. La technologie de l'électroluminescence se développe mais elle est encore assez coûteuse surtout pour le développement de laboratoires scientifiques qui mènent des recherches en photovoltaïque. L'électroluminescence nécessite un peu de temps pour fournir un large éventail d'informations sur le module photovoltaïque mesuré.

L'objectif de ce travail est d'utiliser une caméra commerciale pour effectuer une électroluminescence sombre Les mesures ont été effectuées sur différents modules photovoltaïques (multicristallins et monocristallins) à différents réglages de caméra tels que les variations du nombre f, les vitesses d'obturation et à différents courants de court-circuit et les résultats obtenus ont été utilisés pour prouver expérimentalement le théorème de réciprocité de Rau.

Il est en effet prouvé que les cellules/modules solaires avec une tension de circuit ouvert (COV) plus élevée ont une EQE à efficacité quantique d'électroluminescence plus élevée. Pour chaque augmentation de 60 mV de la tension en circuit ouvert, l'efficacité quantique de l'électroluminescence augmente d'un facteur dix.

Le projet est en mesure de donner une approche expérimentale du Théorème de réciprocité de Rau et de créer une configuration abordable pour les mesures d'électroluminescence.

Mots clés: Efficacité quantique de l'électroluminescence, théorème de réciprocité, modèle de caméra, luminosité de l'image par électroluminescence et tension en circuit ouvert.

INTRODUCTION

1. Background

Today, electricity serves as the primary source of energy for practically every industry that supports human life. Rapid urbanization and industrialization have increased the need for power, which has resulted in an over reliance on conventional energy sources. Global warming and other problems are starting to be caused by over usage of traditional energy sources. We so require alternative energy sources that do not contribute to global war**ming** (Baghel & Chander, 2022)**.**

The IPCC Special Report on Global Warming of 1.5C shows that warming due to anthropogenic GHG emissions from the pre-industrial era to the present will remain for centuries, and will continue to cause further long-term changes in the climate system. Climate change mitigation has become one of the most critical global policy challenges as it requires a coordinated international and local initiative (*Dioha & Kumar, 2020).* As the growing transition to renewables continue, solar has been at the forefront due to its reduced cost compared to other renewable sources *(Africa Has the World's Most Potential for Solar Energy | World Economic Forum.).* It is therefore necessary to maximize the potential of the production with photovoltaics. Photovoltaic cells are designed to efficiently absorb light and transform it into energy.

Bell Telephone researchers created the first usable PV cell in 1954. PV cells were employed to power U.S. space satellites starting in the late 1950s. PV panels began supplying electricity in off-grid, or distant, areas without electrical power lines by the late 1970s. Photons, or solar energy particles, make up sunlight. The energies of these photons, which correspond to the various sun spectrum wavelengths, vary. While discovering other ways to harness this energy solar cells were produced. Solar cells or photovoltaic (PV) cells are non-mechanical devices that use sunshine to generate energy. Some PV cells can generate power from artificial light.

Semiconductors are used to construct a PV cell. Photons may bounce off a PV cell, travel through the cell, or be absorbed by the semiconductor material when they hit the cell. Only the photons that are absorbed have the energy needed to produce electricity *(Photovoltaics and Electricity - U.S. Energy Information Administration (EIA)).*

Crystalline silicon solar cells, which were descended from space solar cells, were hopelessly expensive as a source of terrestrial energy and that some new, groundbreaking technology, typically envisioned to be a thin film, but sometimes as a concentrator, would quickly emerge

and dominate, leaving crystalline silicon for space applications only, at the time of the birth of the terrestrial photovoltaic industry in the mid-1970s.This was a foregone conclusion since, at the time, it was clear to the majority of people that the process was too costly to be a reliable source of energy outside of isolated, low-power applications *(Swanson, 2006).* Crystalline silicon is now an unavoidable low-cost source of power because to remarkable advancements achieved throughout the production process over the past few decades. roughly 700 GW of c-Si modules have been deployed altogether, accounting for roughly 125 GW of the photovoltaic (PV) industry in 2020. By 2040–2050, there are several compelling reasons to believe that c-Si photovoltaics will overtake all other sources of power in the globe. *(Ballif et al., 2022)*

From comparisons of the physicochemical parameters, macrostructure, and microstructure, the advantages of monocrystalline silicon cells include their flawless lattice structure, high material purity. Its efficiency is between 15-25%, while that of polycrystalline is between 14-17% *(Monocrystalline vs. Polycrystalline Solar Panels (2023 Guide*)). In addition, monocrystalline modules exhibit strong aesthetic value because to their uniform color and lack of spots. Monocrystalline and polycrystalline modules are mostly utilized in rooftop or ground photovoltaic systems *(Xu et al.,2018).*

Faults have been one of the major causes of reduced optimization of production with PV panels. These faults range from those that can been seen with our eyes to those that our eyes cannot see. It has become of importance to regularly check for these faults so as to attend to them as soon as possible.

The main components of a solar power generation system are photovoltaic cells and modules. Defects like fragments, broken grids, and hidden cracks are prone to develop during production, transportation, or application; these not only result in production waste but also lower power generation efficiency and may even cause serious accidents if excessive heat from equipment damage builds up inside the panel.*(Zhang et al., 2023)* The phenomenon of light emission from a photovoltaic panel is known as electroluminescence it happens when a photovoltaic cell or panel is exposed to an electric field or current. Various technologies, such as light-emitting diodes (LEDs), organic light-emitting diodes (OLEDs), and electroluminescent displays, frequently exhibit it *(2012 Defect Detection in Modules with EL).* Electroluminescence is being incorporated into the manufacturing process, installation, and continuous monitoring of module deterioration; electroluminescence is a crucial component of PV module quality testing *(Mccleland et al. 2021).* In its most common form,

electroluminescence is the non-thermal emission of visible light from a crystal (or a system of microcrystals) as a result of current flow. The phenomenon was originally discovered by Lossew. ((*Henisch et al., 1965)*The photographic surveying of electroluminescence (EL) under forward bias was proved to be a powerful diagnostic tool for investigating not only the material properties but also process induced deficiencies visually in silicon (Si) solar cells *(Fuyuki & Kitiyanan, 2009)*One of the most important functions of electroluminescence is to obtain crucial information of PV in a short period of time *(Drabczyk et al., 2016)*A relatively easy-to-use but effective method for learning important details about the performance of photovoltaic (PV) devices is electroluminescence (EL) imaging. EL pictures frequently serve as a kind of X-ray into PV devices, revealing details that are hidden from view. The state of the art for EL image analysis has advanced greatly thanks to the work of several organizations. *(Colvin et al., 2022)*

2. Problem Statement

As the world is moving towards renewable energy one of the major areas, we would look at ways to maximize profit which can be in the aspect of quality assurance and to what depth we can maximize and optimize the production of energy and operation of renewables. This masters thesis specializes in photovoltaics (solar), one of the ways to optimize production from PV is to ensure that our panels are operating optimally. Some panels and cells have cracks and faults that are not visible to our eyes but with the help of an equipment we can see/ detect these faults.

The primary source of information for fracture identification is solar cell pictures. However, the wafer surface does have a few minor fractures. It is challenging for the traditional CMOS camera to effectively record fracture information in the visible light spectrum. Thus, we use electroluminescence (EL) imaging to capture pictures of the solar cells. *(Chen et al., 2019)*

We can detect these faults through several methods, but we would be looking at a way to detect these faults through an electroluminescence test. Electroluminescence test is one of the fastest methods to detect these faults. One of the drawbacks of an electroluminescence test is the cost of the camera used to carry out this test.

3. Research Question

i. What is the cost of carrying out an electroluminescence test using an ordinary camera and changing the filters as compared to using an electroluminescence camera?
ii. What is the difference in quality of images produced by the ordinary camera?

iii. Can this setup be easily used in laboratories?

4. Research Hypothesis

Electroluminescence measurements can be done with commercial cameras at night when changes are made to the camera filters.

5. Objectives of Study

The main objective of this study is to reduce the cost of the camera used to carry out an electroluminescence test in the dark. The cost of an electroluminescence camera spans from €12,000 and above while I will be using a commercial camera of €850 to carry out this test.

Other subobjectives include:

- To prove an experimental approach to the reciprocity theorem
- To increase solar farms reliability and improve maintenance structure.
- To reduce maintenance cost for Solar power plants.
- To aid as an apparatus for research in this university.

6. Significance of Study

This study is significant to help research institutes, businesses and university laboratories carry out electroluminescence test with a customized Digital Single-Lens Reflex (DSLR) CMOS canon 4000d camera that could offer a practical approach while maintaining high-quality photographs using brief exposure periods *(Colvin et al., 2021).*While saving cost this research ranges can help people develop an intuitive knowledge how to take EL images with this camera. This study will also prove the reciprocity theorem which relates the spectral and angular dependences of electroluminescence to the spectral and angular dependencies of quantum efficiencies of a photo carrier collection*(Rau, 2007).*

6. Structure of The Thesis

This study is made up of three main chapters preceded by a general introduction and ends with a conclusion. It is organized as follows: The introduction supplies the necessary background or context. Then, the first chapter is the literature review part. Afterward, the second chapter highlights the materials and methods used in this study while the last chapter presents the results and discussion.

CHAPTER 1: LITERATURE REVIEW

1.1 General aspects:

Measurements of the current voltage (IV) characteristic of a photovoltaic (PV) device are important in determining its total performance and efficiency. Even though the IV characteristic can be used to identify a faulty device under test (DUT), it does not reveal any details on where the fault in the solar cells is situated. Unlike IV measurements, spatial characterisation tools such as luminescence imaging give more details to these faults *(Bliss et al., 2015).*

Although electroluminescence has long been employed in lighting applications and has only lately been added to the list of methods used to test photovoltaic equipment. It involves giving the module a direct current and using an infrared-sensitive camera to measure the Photoemission. The open circuit voltage distribution, minority carrier diffusion length, series resistance, quantum efficiency, and ideality factor of the investigated cell are all correlated with the brightness distribution on the photographs of the cell *(2012 Defect Detection in Modules with EL.).*

The photographic surveying of electroluminescence (EL) under forward bias was proved to be a powerful diagnostic tool for investigating not only the material properties but also process induced deficiencies visually in silicon (Si) solar cells *(Fuyuki & Kitiyanan, 2009).*

Electroluminescence EL imaging is a powerful tool for characterizing defects such as localized shunts and top electrode sheet resistance in solar cells.1,2 EL images have been used to characterize thin film solar cells such as CuIn, GaSe2, CIGS and CdTe *(Brown, 2010).*

Luminescence imaging has become essential for non-destructive characterization of photovoltaic (PV) modules at various stages throughout their fabrication and deployment. In addition to locating cracks and electrode faults, the utility of luminescence imaging stems from the reciprocity relation correlating a material's radiative efficiency with its ability to generate photovoltage and current *(Sulas et al., 2019).*

A way in which electroluminescence test can be carried using a simple digital camera is discussed below.

1.2 Electroluminescence Spectrum of Silicon

A photovoltaic solar cell or panel can be quickly characterized using electroluminescence, and micrometer-scale flaws can be seen easily *(Ahanogbe et al., 2022).* Electroluminescence is the resonant optical radiation emitted in a limited band when an electric current flows through

some substances e.g silicon. In order for this to happen, consider a standard semiconductor with a p-n junction where p represents the positive carriers (holes) and n represents the negative carriers (electrons). The electroluminescent photon is emitted when a voltage is applied across both electrodes, which excites the hole and causes it to recombine with the electrons and fall to a lower energy level as seen in figure 1 *(mix-den: electroluminescence and diode lasers,2019).*

Photoluminescence is the term for the spontaneous light emission from a substance when it is excited by light *(Cordero et al., 2016).* Similar to photoluminescence, electroluminescence (EL) is often measured on completed devices. However, electroluminescence produces extra carriers by current injection, while photoluminescence electrons are excited by light.

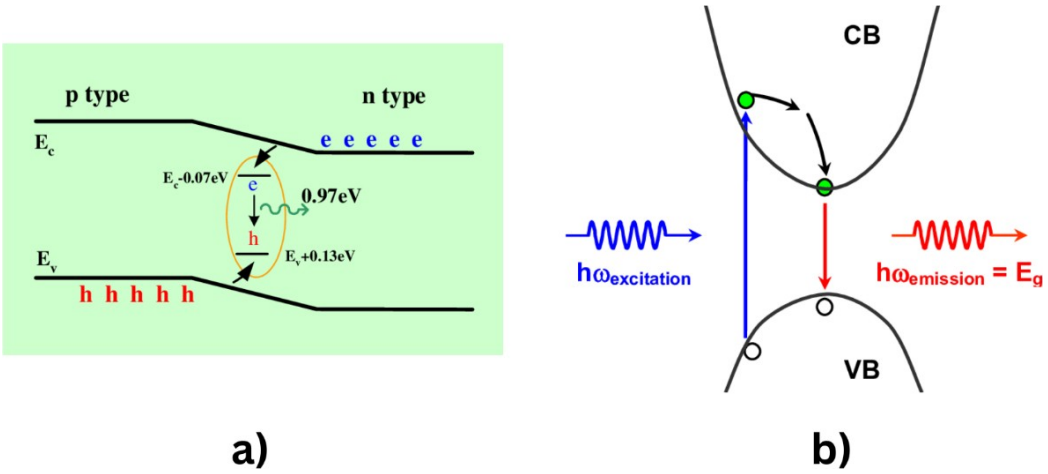

Figure 1: a) Electroluminescence & b) Photoluminescence. *(Ye et al., 2014; Yoshikawa et al., 2017)*

Figure 1 shows what occurs in a solar cell for photoluminescence and electroluminescence to be produced. For photoluminescence the incident light excites the holes from the valence band(VB) and the move to the conduction band (CB) and gains electrons, after it tloses the excess energy and as it returns to the lower energy level it emits light.

When compared to direct bandgap semiconductors like gallium nitride (GaN) or gallium arsenide (GaAs), silicon, which has limits in effective light emission, is a semiconductor with an indirect bandgap. But there has been progress in understanding the electroluminescent characteristics of silicon-based products and materials.

Electroluminescence has a more rapid response as compared to photoluminescence, both phenomena are used in explaining the light phenomenon of a solar cell, for the purpose of this thesis electroluminescence will be discussed.

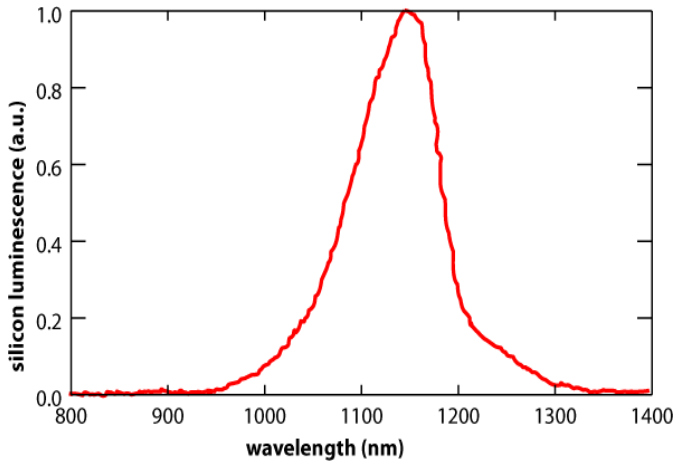

Figure 2: Electroluminescence of Silicon *(Ciocia et al., 2019)*

In accordance with its bandgap, silicon's electroluminescence peaks at around 1150 nm, as seen in **Figure 2**. Electroluminescence takes about one second. This luminescence is a rather accurate and non-destructive method of measuring a silicon wafer *(Ciocia et al., 2019).*

CHAPTER 2:MATERIALS AND METHODOLOGY

In this Chapter, we discuss the different materials and the methodology used during the process of the thesis.

2.1 Electroluminescence detection setup

Figure 3 show the schematic setup for the dark electroluminescence experiment carried out in this thesis. The solar panel under test is connected to the power supply, a temperature sensor is connected to the module and to the laptop to monitor the temperature changes. The camera is placed on a tripod at a given distance from the module and the electroluminescence images are taken. The specifications of each of the equipment are discussed in details in subsequent chapters**.**

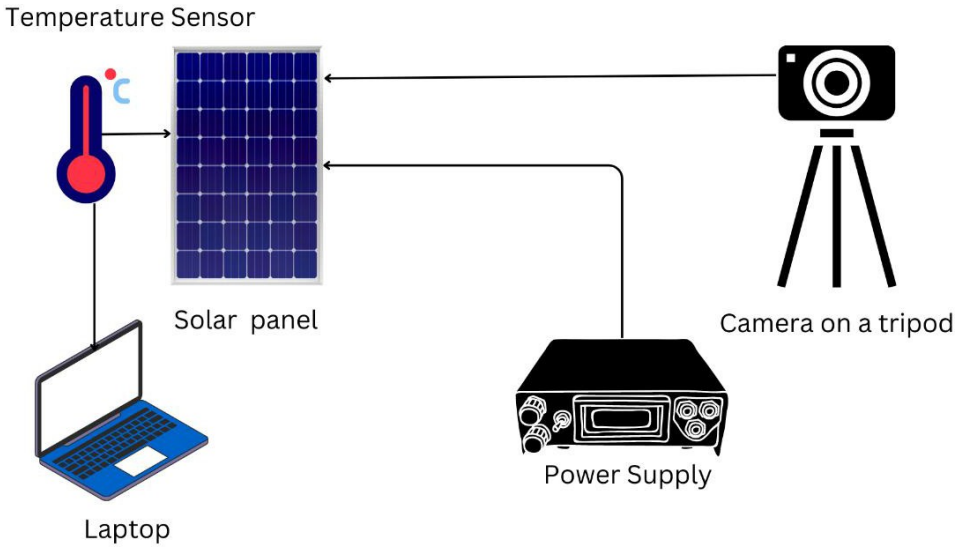

Figure 3: Setup of the project.

Figure 4 shows how the real setup appears.

Figure 4: Real Setup of The Electroluminescence Measurement.

An electroluminescence setup based on commercial digital camera was developed. The acquisition of electroluminescence images on both monocrystalline and polycrystalline silicon solar cells showed that the detection of differing types of defects in solar cells is possible *(Frazão et al., 2017)*. The measurement of this thesis is targeted towards silicon solar modules and how the camera responds at different settings. The measurements were done with the help of the following items.

- Camera
- Filters
- Power source
- Temperature sensor
- Modules
- Software

2.1.1 Utilization of a commercial camera for measurement

The action of charge integration on a p-n junction was proposed by Weckler in 1967 and is regarded as the core principle of complementary metal oxide semiconductor (CMOS) image sensors. Modern CMOS image sensors have surpassed charge coupled device (CCD) camera in the majority of sectors. A wide range of functionality, quick readout, low power consumption, low cost, and some improved characteristic qualities are offered by CMOS image sensors as an integrated technology *(Jain, 2016).*

Figure 5 illustrates the working principle of a CMOS camera. The camera operates a pixel parallel digital (PPD) system, which consists of photodiodes and pixels organized in a grid pattern, it absorbs the photons. The photodiode transforms the photons (incident light) into electrical impulses when it strikes each of the grids. These electric signals are then sent to the charge to voltage circuit which converts the electrical impulses to voltage and the voltage is amplified at system gain and sent to the analog to digital converter, which converts the voltage to digital values that represent the brightness or intensity of each image seen *(Jain, 2016).*

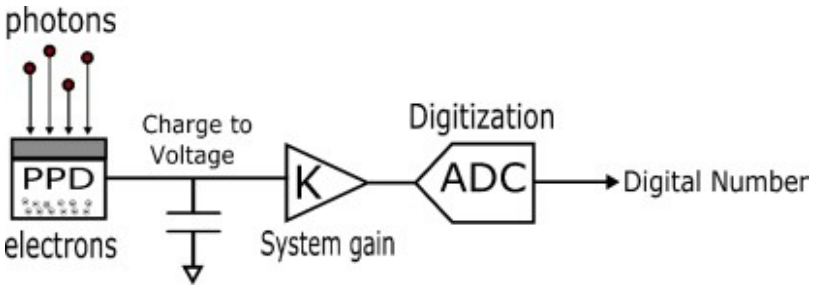

Figure 5: Working Process of A CMOS Camera *(Jain, 2016).*

Applications that require high-sensitivity, low-noise cameras at an affordable price point with quick data transfer rates are perfect for CMOS cameras. These cameras offer high-definition photos for a variety of applications and utilize the newest CMOS sensors. The camera is being modified as the details will be explained in subsequent chapters, the resolution permits to acquire small details of the solar cells (such as cracks and the consequent edges of broken cells), while a high ISO sensitivity value could be useful in case of low emission from the PV generators *(Zhang et al., 2023).*

2.2 Canon EOS 4000d

Figure 6 shows a picture of the camera used in this thesis, it is a normal CMOS 18 mega pixel camera. CMOS-based imagers have important advantages over CCDs, such as system-on-chip capabilities, reduced power consumption, and perhaps cheaper cost. Compared to current CCD cameras, which need several support ICs and discrete components, the eventual single-chip consumer camera is less expensive *(Lulé et al., 2000).* The cost oof the camera used in this thesis is €850. The filter used on this camera is a Heliopan ES RG850 visible ray blocking filter. It allows only infrared signals into the camera

Figure 6 : Canon EOS 4000d Camera.

.

The pictures gotten from the camera are in a CR2 format and for these results (pictures) need to be properly analyzed by fiji the analyzing tool used in this thesis. The pictures are converted from CR2 files to Tagged Image File Format (TIFF), to analyze the electroluminescence intensity accurately without masking the values. The pictures were taken in portrait mode to maximize the number of pixels being used since the panel is held in a portrait mode by the panel stand, as seen in **Figure 4**.

Figure 7 depicts the sensitivity of a CMOS and CCD camera sensor with the black curve, it also displays the sensitivity of the colors with in a normal camera with an infrared blocking sensor (the light blue line). It shows that the filter only allows the colors to show in the visible and blocks light from the infrared wavelength. The graph also depicts that the red blue and green channels are still open at the infrared wavelength. If pictures are taken in this wavelength they would not be pleasing to the eye as our eyes are only sensitive in the visible regime from 400 to 750nm. If one removes the IR filter and does not replace it with another filter the camera receives data from 2 > 800nm.

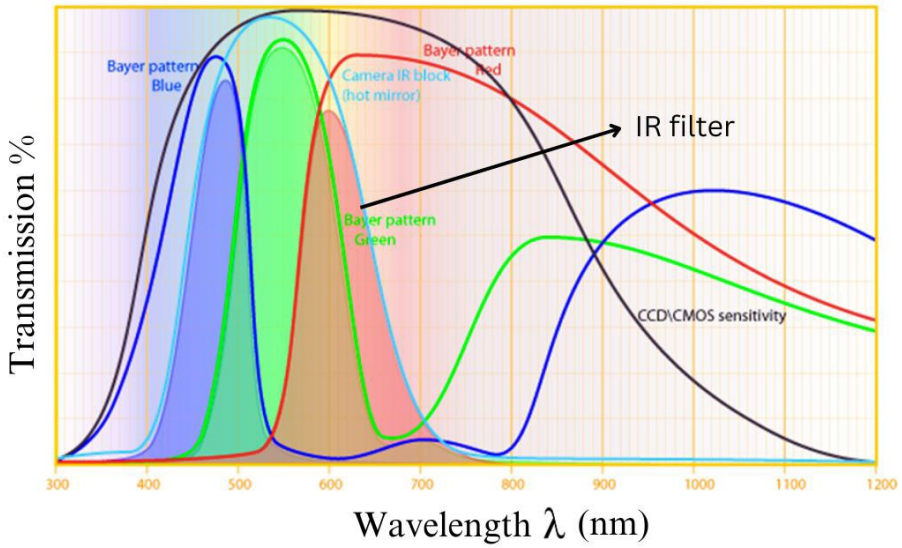

Figure 7:Transmission Curve Filters And Sensors Channels Of A Camera *(IR-Photo.Net | Infrared Photography.).*

2.2.1 Camera modifications

The compromise involved in electroluminescence (EL) imaging must be balanced. When choosing a camera, factors including signal to noise ratio (SNR), file size, feature visibility, resolution, and hardware cost must be taken into account. Although these factors have an influence on image quality, it is still unclear how much of an impact they truly have.

The effect of the parts and camera settings further complicates this. The following factors also affect image quality: distance, tilt, background noise, ISO, lens diameter, focus, f-number, and exposure duration. Images may be processed with basic approaches to account for these factors.

2.2.2 Filters

For normal pictures an Infrared Cut/Blocking Filter is built into camera sensors to filter out undesired IR radiation as illustrated by the light blue line in figure 7. The IR Cut/Blocking Filter is removed from this CMOS Sensor while an IR Filter which filters out all data < 850 nm is installed on the lens of the camera used.*(Numerical Study of a Steam Methane Reformer Integrated Membrane System for 250 Kg/Day Hydrogen Production, 2022).*

The filter in **Figure 8** is the Heliopan 28mm RG 850 Infrared Filter, as it allows roughly 85% of infrared light > 850nm or more through

Figure 8: Heliopan RG850 Filter.

Figure 9 displays the transmission curve of the filter. In short wavelengths it has close to zero transmission but in long wavelengths it has high transmission.

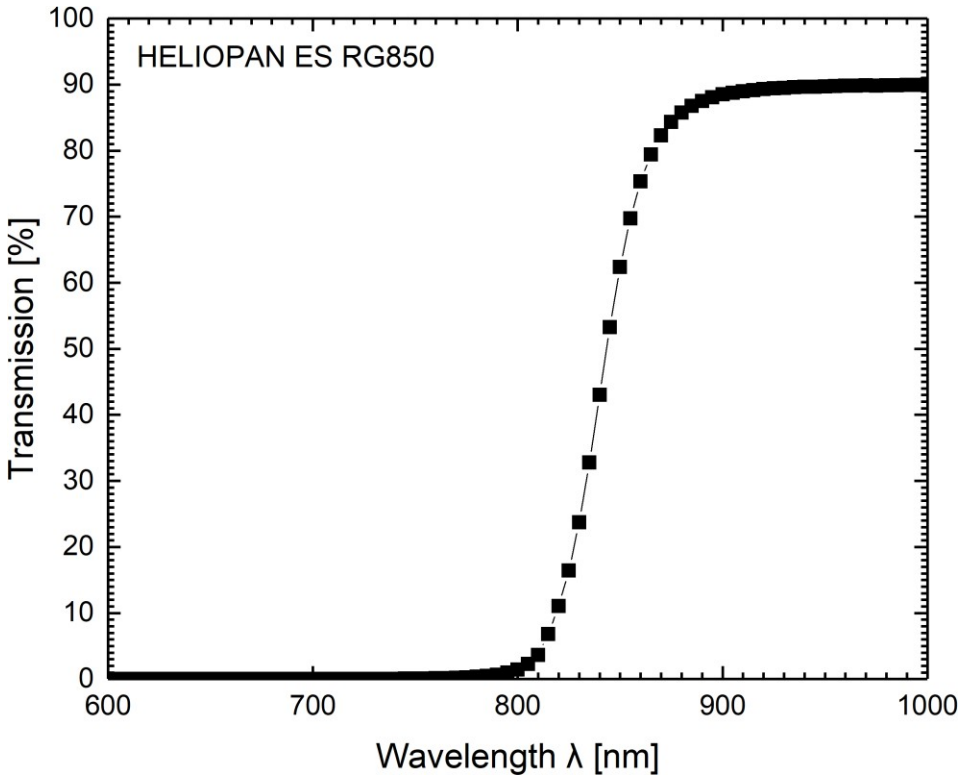

Figure 9: Measured Transmission curve of the filter used.

2.2.3 Transmission test

Figure 10 shows the UV vis spectrometer used to carry out this test. The process of operation of this equipment is to supply photons(light) on the material to be measured and compare the number of photons(light) that pass through or how much gets reflected to that which is obtained from the reference material over different wavelengths based on the person's interest. This equipment makes use of tungsten and deuterium lamps.

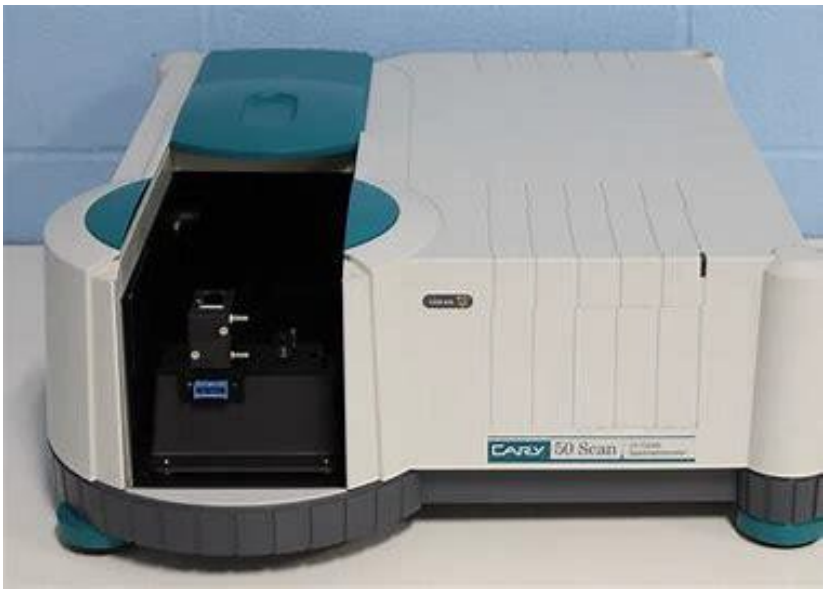

Figure 10: UV VIS Spectrometer.

The process starts by switching on the UV vis spectrometer and allowing it to initialize that is allowing it to warm up before starting up the software, this process takes about ten minutes. The next step will be to start the UV wavelab software which helps us select the range we would want and also to view the graph plotted by the information gotten by the sensors in the machine. After confirm that the system is ready, a reference (test run) of the filter measurement is carried out at 100% light and at 0% light. The filter is then placed in the measurement space and the test is ran and the software gives both a graph and an excel sheet of all data point to help carry out any other calculations needed. The measurement of the filter was done from 300nm to 1200nm and a timing interval of 5nm was used. The result gotten is plotted in **Figure 9**.

2.2.4 Camera Calibrations

A pixel is the smallest unit of an image *(Bedrich et al.)*, it is the short form of the word picture element. A pixel can also be said to be a square filled with colors. This square is divided into 3 colors, Red, Green and blue, these colors are combined and used to produce the different

colors the eye reads. The camera always tries to produce an image that can be appealing to the eyes.

Images of electroluminescence cannot be seen by our naked eyes but with the help of a camera that tends to make this image in a pleasing manner to the eyes. The images have 3 channels as the red green and blue channel are also open in the infra-red. The camera was set in raw file mode, and an 8bit image that provides images for each pixel with brightness values from 0 to 255. The brighter the image gets the more filled our pixel pocket gets. Above a certain point the pixel is full, the sensor gets into saturation.

2.3 Camera Settings

2.3.1 Shutter time t_s

The exposure time controls how much light comes in. To lessen camera blooming, which is a result of overexposure, shutter speed or light levels can be changed. By increasing the shutter speed, it is possible to take images faster like cars driving past or of picture of things in motion. In essence, it's the time it takes for a camera to capture a photo.

The shutter speed has an effect on the brightness of the image produced. Fast shutter speed produce not so bright electroluminescence images but longer shutter speed produce brighter electroluminescence images.

2.3.2 F-number f_N

The F-number f_N is defined via

$$f_N = \frac{f}{d}, \tag{1}$$

where f is the focal length of the camera, and d is the diameter of the iris. The area A_s of the iris is

$$A_s = \pi d^2 , \tag{2}$$

Therefore, it holds that

$$A_s = \pi f^2 / f_N^2, \tag{3}$$

Typical F-numbers are f_N = 1.4, 2, 5.6, 8, 11, 22. Our camera allows F-numbers of f_N = 2.8, 3.2, 3.5, 4, 4.5, 5.0, 5.6, 6.3, 7.1, 8.0, 9.0, 10, 11, 13, 14, 16, 18, 20, 22.

Sometimes F-numbers are also characterized by the diameter and written as f/5.6, f/2.0 etc. In other cases (like in **Figure 11**) they are also given by f1.2, f2.8, f4. etc. We have to consider that, when calculating the diameter of the iris.

As a consequence of **Eq. (3),** the F-number f_N via the area A_s of the iris, controls the amount of radiation that falls on the sensor of the camera.

Figure 11 gives an overview of what the different F-number gives the size of aperture for a picture. It shows that the larger the F-number, the smaller the open iris area (Kelby, 2013) .

Figure 11 : F-Numbers and Area of The Camera Iris *(Which Aperture Is Best for Portraits or Landscape.)*

2.3.3 ISO value

"International Organization for Standardization" is known by the abbreviation ISO. Camera ISO does not, however, specifically relate to the body that develops various technological and product standards. Since two film standards known as ASA and DIN were unified as ISO standards in 1974 (later amended for both film and digital photography), they have always been referred to as "ISO" standards. Although ISO initially exclusively described film sensitivity, digital camera makers gradually embraced it with the aim of preserving brightness levels comparable to film. A camera's "base ISO" is the lowest native ISO setting available. This option is crucial because it enables one to get the best possible image quality while limiting the visibility of noise as much as possible. Some ranges include ISO100, 200, 400, 800, 1600 & 3200.

2.4 Power Supply

The power supply used is to drive electric current through the photovoltaic modules. The power supply used here is the Delta Elektronika CVCC (Constant-Voltage-Constant Current) Maysun MS410MB-40H. With its precise control over the voltage and current it makes it suitable for our project (Home | Delta Elektronika.).

Figure 12 displays the power supply (delta electronica SM70-22) used in this thesis. This equipment is able to supply the different modules with the needed direct current and voltage

without flickering effect. It was chosen due to the range of the open circuit voltage and short circuit current of the panels that will be measured. It is easy to control, this is because the power supply makes use of a control loop, if controlled by the current once the current is set the voltage increases or decreases concurrently to produce the desired current being programmed. The power supply will switch from voltage regulation to constant current mode when the load current gets close to the predetermined maximum limit. By doing this, one can be confident that the power supply will safeguard the load against excessive current draw and guard against harm to the load or the power supply.

It gives precise readings from the LED as this would help to know the precise voltage and current sent into the panel so it would be easy to compare between different panels.

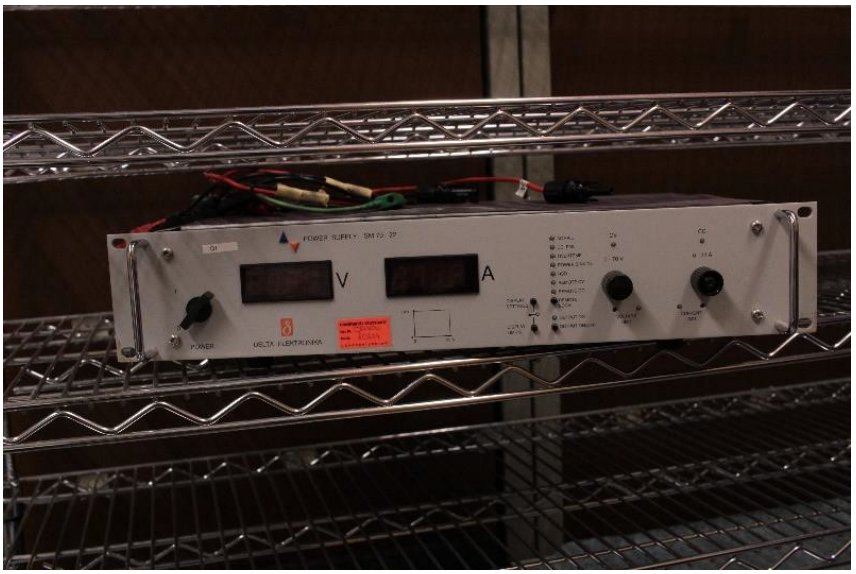

Figure 12: Delta Elektronika Power Supply**.**

2.5 Temperature Sensor

Figure 13 displays the PT100 (platinum100) temperature sensor is used during the measurements. We employ a temperature sensor because it is important for the experiments' purpose to understand how temperature affects the results we are receiving. This provides us with the panel's immediate temperature change per second. A computer's PUTTY program displays the temperature with the help of a Max31865 STM microcontroller that is able to convert the data gotten from the temperature sensor and produce signals that our computer is able to understand and display the different temperatures in degree Celsius. During the various measurements, the temperature sensor was fastened at the back of the panel at the center of a

cell to monitor the changes in temperature changes. The temperature changes during the experiments increased as we increased the input current increased. The difference between each measurement was about 1 degree. These changes had no major impact on the electroluminescence images taken. **Table 1** shows the typical temperature ranges of an electroluminescence measurement.

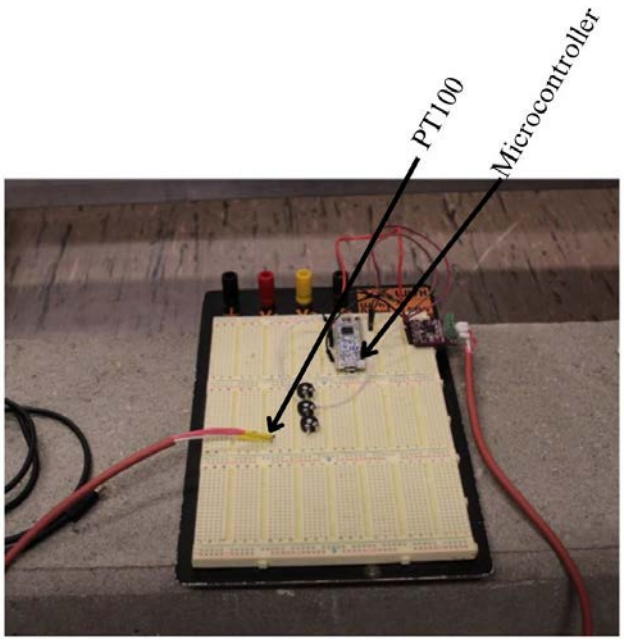

Figure 13: PT100 and The Microcontroller.

Table 1: Measured Values of Trina Electroluminescence Test Showing the Temperature Changes.

CURRENT [A]	SHORT CIRCUIT PERCENT I_{SC} [%]	VOLTAGE [V]	TEMPERATURE [ºC]
1.2	10	38.8	26.1
2.4	20	39.2	26.2
3.6	30	40.3	26.5
4.9	40	41.2	26.8
6.1	50	41.9	27.5
7.2	60	42.4	27.7
8.5	70	43.0	28.2
9.8	80	43.5	28.9
11.0	90	43.9	29.6
12.2	100	44.5	30.5

2.6 Photovoltaic Modules

Table 2 gives a list of the different photovoltaic modules used and their characteristics. The different panels used in the process of this thesis were chosen to show the differences in electroluminescence in different modules, and show that even if they have similar characteristics there can still be differences the electroluminescence produced. Some of these changes are due to factors like the cell technology, some faults on the panel etc.

Table 2: List of Panels Characteristics.

Brand of Module	**Name of module**	**Type of module**	**Nature of strings connection**	**Total number of cells**	**Cell [cm^2]**	**Efficiency [%]**	**Open circuit Voltage V_{OC} [V]**	**Short Circuit Current I_{SC} [A]**	**Field factor [%]**
Maysun	MS410MB-40H	Mono-crystalline	80 cells in series	80	220.5	21	53.2	9.8	78
Trina	TSM-400DE09.08	Multi-crystalline	60 cells in series (2 strings) and 2 in parallel	120	147	21.1	41.4	12.3	79
Sun power	SOR-225-WHT-1	Mono-crystalline	72 cells in series	72	156.3	18.1	48.5	5.9	79
Sun Electronics	SV-X-210-FA1	Multi-crystalline	38 cells in series (3 strings) and 3 cells in parallel	114	120	13.8	23.1	12	75
Chinalight	CLS-230P	Multi-crystalline	60 cells in series	60	240.3	14	37.4	8.3	74
Yingli	YL225-29b-1	Multi-crystalline	60 cells in series	60	225	14.1	36.5	8.2	74

2.7 Softwares

2.7.1 Softwares For Brightness Measurements

Fiji also known as “Image J” is an image analysis and processing software that includes a number of plugins that make it easier to analyze scientific images (*Schneider et al., 2012*). The Image J version 2 is the version of Image J used in this thesis, the software provides features such as macros that aid in carrying out recurrent task when using this software. This was utilized when converting the different electroluminescence images from CR2 raw files to tagged image file format (TIFF).This was done by uploading a macro script that would subtract the electroluminescence image from the background image and saving it as TIFF using the functions of the software so this can be done for multiples of image. This TIFF is then opened using the Image J and an average bright cell is selected and measured using the measure function on the software and the results gotten can be saved as an excel file. Images in TIFF are easier to analyze as they contain the data that was taken by the image and not being changed. The software has the measure feature that aids in giving numerical values to the brightness of the images taken. It also offers the option that you can view the brightness of an image with a histogram to see when the image gets into saturation.

Figure 14 shows how the cell of the modules are measured to derive the electroluminescence brightness of the module.

Figure 14: Measurement of El of a Cell with Image J.

2.7.2 Software For Data Plotting

The OriginLab Corporation created the robust data analysis and graphing program called Origin. All data analysis and graphing in this thesis were carried out with Origin version 1. its interface and intuitive features were helpful in curve fitting and data uploading.

2.8 Methodology

The methodology used is the forward bias electroluminescence. In this method, current is passed through the terminals of the panel, and electroluminescence is emitted and with the commercial camera the electroluminescence measurements are taken. This is done at different currents and different settings of the camera. The different currents used are from 10% of the short circuit current to 100%. The results gotten will be discussed in this chapter.

2.9 Processing

Electroluminescence of a solar cell is measured when the voltage is applied on the solar module, a picture of the module is taken. The image gotten is then processed using an analytical software to measure the brightness of a cell in the panel. After each electroluminescence image is taken, a background picture of the panel is also taken. The background image is subtracted from the electroluminescence image, this is to take out dark current or background noises. After the images are subtracted, they are converted to a tiff file. The resultant image is measured by selecting an average cell on the module and the value gotten by measuring this cell with the help of the Image J software is the electroluminescence value of the module, the EL brightness B.

CHAPTER 3 RESULTS AND DISCUSSION

3.1 Preliminary results

Figure 15 shows the raw electroluminescence image of a monocrystalline Trina module and the background image before their conversion to TIFF. The reason for the pinkish color seen despite the camera being set to monochrome is because the image is a raw file and it would take the closest color available to it which is the red.

To start out this procedure we carried out the electroluminescence test of a Trina TSM-400DE09.08 monocrystalline silicon solar module which has 120 half cells. This test was done at different current ranges, from 10% to 100% of the short-circuit current $I_{SC,}$ (see table 1)

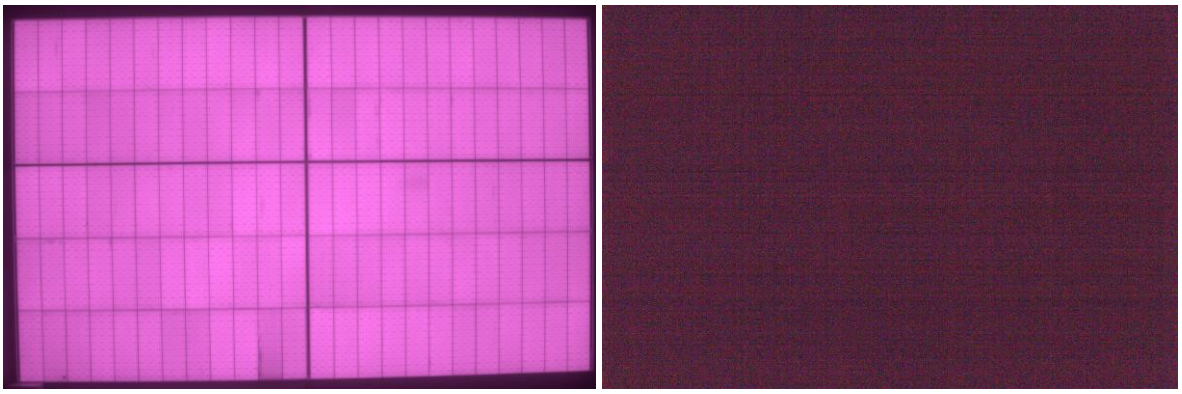

Figure 15: Raw Electroluminescence Image and Background Image of a Trina Module.

Figure 16 shows the cell measured to give the value of the electroluminescence (EL brightness).

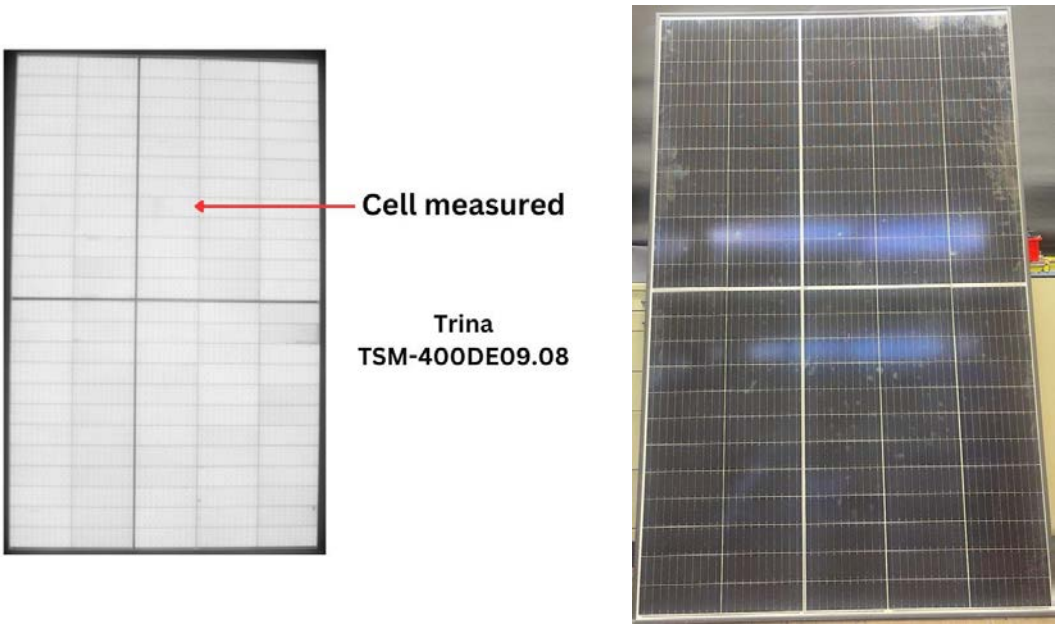

Figure 16: Trina Module Measured for Electroluminescence.

The measured relationship between electroluminescence brightness and current is expressed in **Figure 17.** It is seen that as the current increases, the brightness of the image increases linearly until at values above 500. For this test the other camera settings are kept fixed: The F-number is at $F_N = 5.6$, shutter time is $t_S = 15$ s, and the ISO is ISO 400. The increase of the measured brightness in **Figure 17** for higher currents is easy to understand. The higher the direct current, the more carriers recombine radiatively per second. Therefore, more photons per second are emitted and measured. As a result, increasing the current I, results in an increase in the electroluminescence's intensity or brightness B.

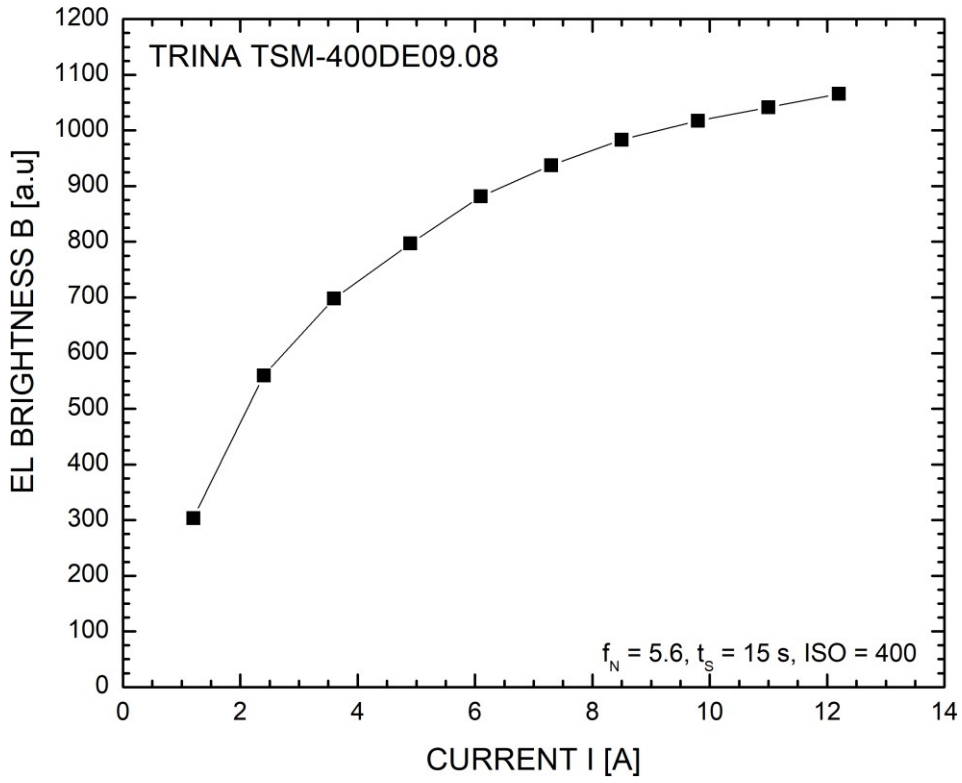

Figure 17: For Low Currents Electroluminescence Increases Linearly. For Currents Above I = 4A, The Electroluminescence Deviates from Linearity and Goes into Saturation.

Table 3 shows the generated values from the elektronika power supply for the current values of **Figure 16** and the electroluminescence values gotten when the cell was measured.

Table 3: Measured Values of Trina Module Electroluminescence Test.

CURRENT [A]	SHORT CIRCUIT PERCENT I_{SC} [%]	VOLTAGE [V]	ELECTRO LUMINESCENCE
1.2	10	37.3	303.6
2.4	20	39.0	559.8
3.6	30	40.1	698.2
4.9	40	40.8	797.1
6.1	50	41.6	881.3
7.3	60	42.2	937.5
8.5	70	42.8	983.3
9.8	80	43.3	1017.3
11.0	90	43.7	1041.2
12.2	100	44.1	1065.5

The link between electroluminescence brightness B and shutter opening time t_S is seen in **Figure 18**. The longer the shutter time the more photons the camera is able to absorb and the brighter the image will be. For short shutter times, we observe a linear increase, but at EL brightness values above 500 the curve goes into saturation. We will show below, that the saturation behavior in figures 17& 18 is not due to the modules but due to the camera sensor. Every sensor has a specific operational limit, which is the point at which the sensor's output signal ceases to respond to input stimuli at a certain level. It refers to the point at which a sensor's output ceases to respond linearly as required to the input stimulus at a certain level.

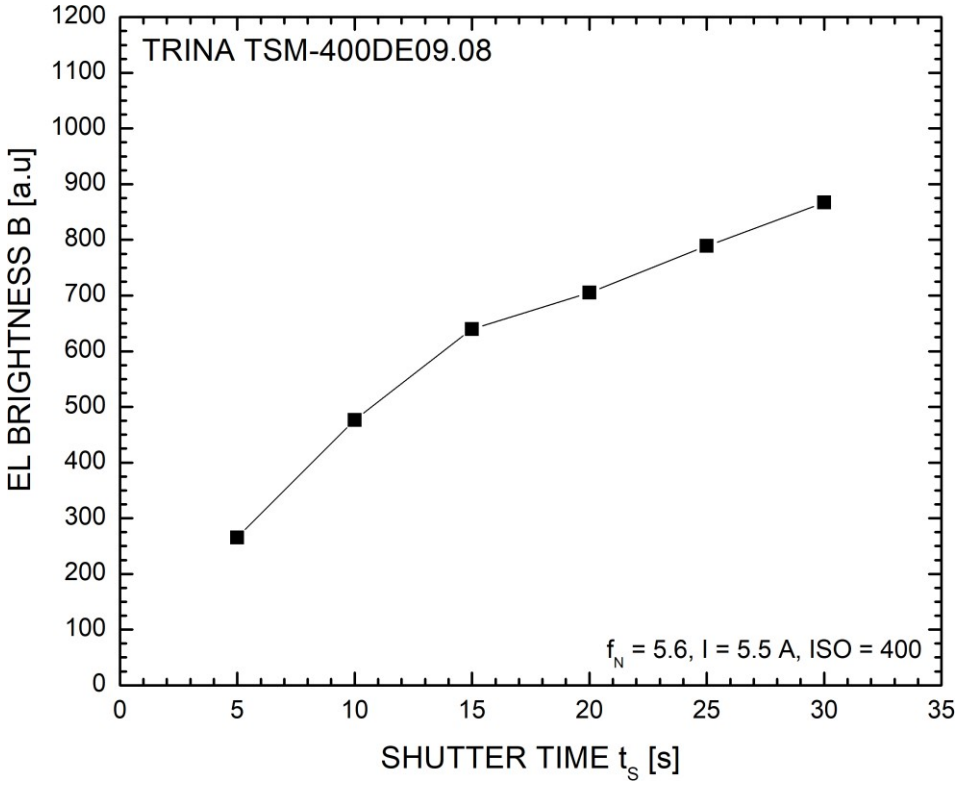

Figure 18: For Long Shutter Times, The Brightness Decreases More And More From A Linear Behavior.

Figure 19 depicts the relationship between the shutter area and the electroluminescence, the shutter area is calculated from the F-number using equation (3). **Figure 19** is produced by passing a current I = 5.5A and keeping the ISO at 400 and a shutter time t_S = 15 s for the Maysun module. The different F-numbers used here are f_N= 3.5, 4, 5.0, 5.6, 6.3, 7.1, 8.6, 9.0 and 10.0.

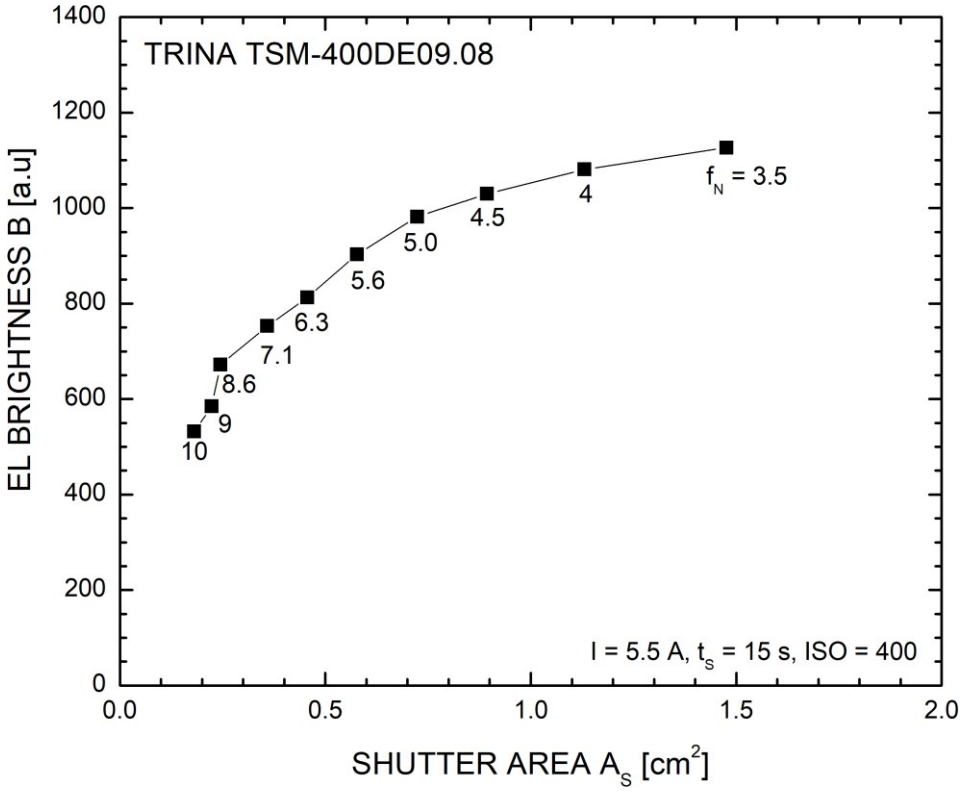

Figure 19: The Saturation Behavior Is Also Observed For Increased Shutter Areas.

The relationship between the ISO values and electroluminescence brightness can be seen in the **Figure 20**. The pixel brightness and photon generated charge are amplified to a certain degree by the ISO setting. The camera's performance is represented by the sensitivity. The ability to distinguish between the signal and the background noise is a part of this. It is possible to increase the sensor's quantum efficiency (spectral band) or reduce the sources of noise in order to increase the signal-to-noise ratio. In **Figure 20** the current is kept constant at 50% of the short circuit current, the shutter time is t_S = 15 s and the F-number of F_N = 5.6 are kept constant. Saturation is also noticed in figure 16 for B > 500 in the y-axis, the graph begins to slant.

The electroluminescence brightness represented in each of the graphs is the summation of the information saved in each of the red, green and blue channels of the camera. **Figure 20** elucidates the relationship between the brightness and product X.

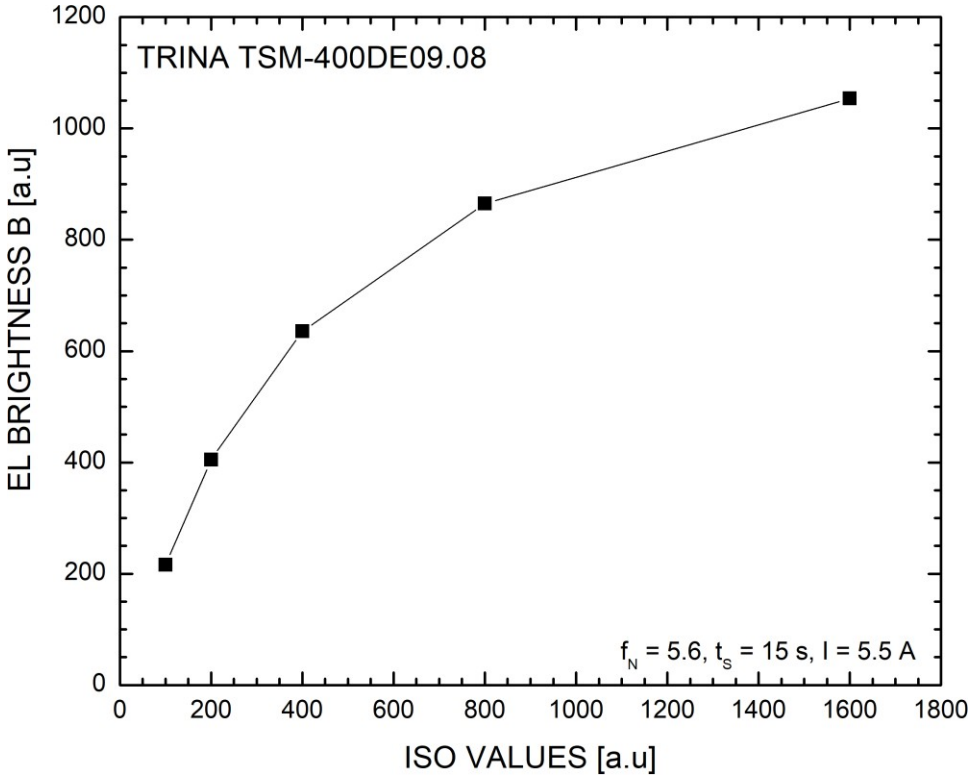

Figure 20: For Larger ISO, Saturation Is Observed.

Figure 21 shows the relationship between the electroluminescence brightness and a product X. Product X is gotten by the multiplication of the varying the current density passed through the module, and shutter time t_S = 15 s, the F-number f_N = 5.6, and at ISO 400. The afore mentioned parameters play an important role in the output image obtained. These parameters can alter how the image would appear regardless of the actual image that is produced by passing a certain amount of current as would be seen in subsequent graphs. From **Figure 19** the saturation of the different color channels is seen. The electroluminescence of the red, blue and green channels is deduced by taking our raw image and measuring the average cell with the Fiji software. From the values gotten it can be seen from **Figure 6** that in the infrared wavelength the red channel's curve is the highest followed by the blue then the green curves, hence the difference in values obtained at each level. The summation of the three channels produces the monochrome curve, this was confirmed by measuring the TIFF of the images and the output was the same as the summation of the three channels at the particular input current. This test was carried out with the Trina TSM-400DE09.08 panel, the curves showing the electroluminescence image brightness begins linearly and goes into saturation above 500 EL for the monochrome, the

saturation for the other curves begin earlier and this can be seen in the graph above that each channel gets into saturation separately and our monochrome graph the summation of all three channels to give us a good curve.

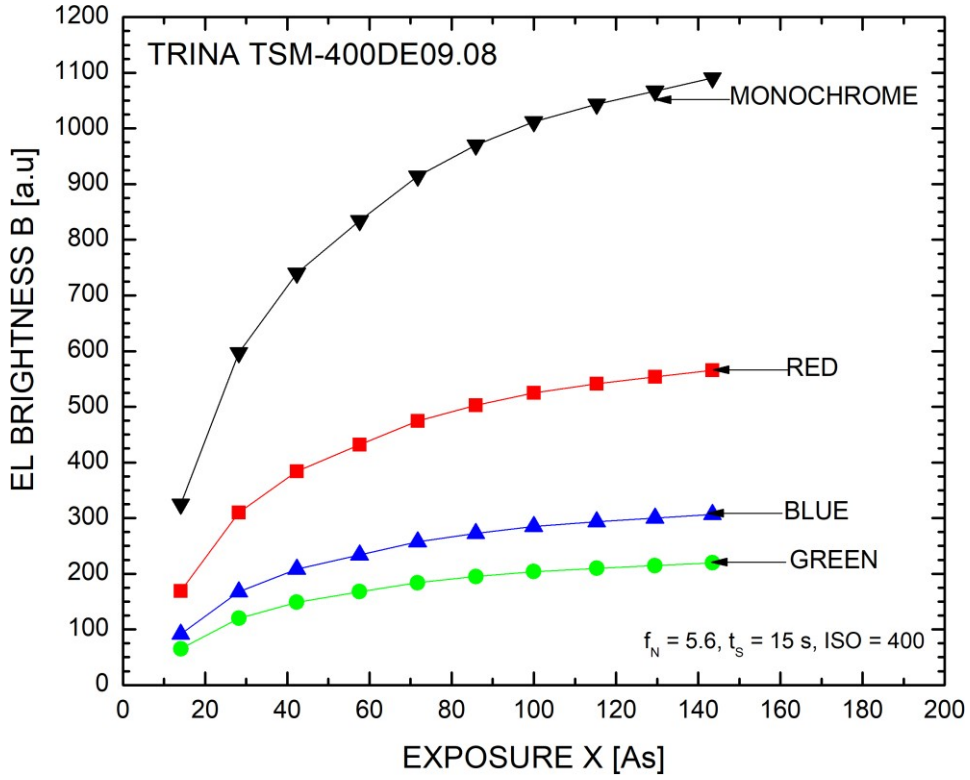

Figure 21: Behavior of Separate Color Channels And Their Summation (Monochrome).

3.2 Electroluminescence Measurements

The measurements for the brightness *B* in Figures 16 to 19 saturate. From Figure 16 alone, one could speculate that for higher currents I, the percentage of electron/hole pairs which recombine radiatively would be lower than for lower currents. However, in Figs. 17 to 19, the currents are kept constant and just the camera settings are changed. For all three figures, the brightness B increases linearly first, then it tends to saturate. Here we show that the observed saturation is not due to physical processes in the measured photovoltaic module but due to the saturation of the camera pixels. However, first we have to explain i) the quantum efficiency EQE ii) how he brightness data are taken. Then, iii) we present a novel, universal brightness and camera model for electroluminescence measurements. This model will be published separately (Werner et. al. 2024).

3.2.1 Luminescence quantum efficiency EQE_{LED}

When the electric current I injects electron/hole pairs in pn-junctions, solar cells or solar modules, those carriers recombine either non-radiatively or via the emission of photons (radiative recombination). The luminescence quantum efficiency EQE is defined as

$$EQE_{LED} = \frac{J_{phot}}{J_e}, \tag{4}$$

where J_{phot} is photon current density which leaves the surface of the device per cm^2 and s in all directions. Note, that depending on geometry, only a part of those photons will be collected by our camera objective. The symbol J_e in Eq.(3) stands for the electric current density. For a module in which all the cells are connected into series, the electric current density is simply given by $J_e = I/A_c$, where I is the injected module current and A_c is the cell area. When several cells or cell strings are also connected into parallel, the current density is given by

$$J_e = \frac{I}{n_p A_c}, \tag{5}$$

where n_p is the number of parallel connected cells or cell strings.

3.2.2 Brightness and Camera Model

3.2.2.1 Brightness parameters

The measured brightness *B* in **Figures16 to 19** depends on several parameters

- The opening time t_s of the shutter: The longer it is open, the more photons are collected.
- The shutter area A_s: Larger shutter areas (smaller f_N-values of the iris) capture photons from a larger solid angle.
- The ISO-value: The higher the ISO-value, the higher is the sensitivity of the camera (chip), achieved by a higher voltage at the pixel sensors or amplifier(s).
- The current density J_e in the module: The higher the current density, the more electron/hole pairs recombine per second within the module and have the chance to emit a photon.
- The (electroluminescent) quantum efficiencyEQE_{LED}: The higher is this number, the more photons are emitted per recombining electron/hole pair.
- The geometry *G* of the set-up: The closer the camera is to the photovoltaic module, the more photons are captured. As long as we keep the geometry constant (and always use the same objective lens for the camera), *G* is expected to be constant.

- The internal conversion C_{int} and storage of electrical data within the camera. Here for example, a saturation of the pixel capacitors by overexposure is possible. As long as there is no overexposure/saturation, C_{int} is constant.
- The external conversion C_{ext} which we use to convert the brightness of the TIFF images into the value B of the brightness. As long as we use always the same settings of the software and try to keep the averaging over cells also always the same, C_{ext} should also be constant.

3.2.2.2 Brightness parameters and exposure X

For the brightness B we write

$$B = G\, C_{int} C_{ext}\, EQE_{LED}\, J_e t_s A_s ISO. \tag{6}$$

As, at the beginning, the parameters G, C_{int}, C_{ext} are unknown to us, we collect them and define their product

$$\alpha = G\, C_{int} C_{ext}\,. \tag{7}$$

We expect α to be constant, as long as the pixel sensors do not get in saturation due to overexposure.

Similarly, we collect also the injected current density J_e, as well as the camera settings t_s, A_s and ISO and define the exposure

$$X = J_e t_s A_s ISO. \tag{8}$$

As a consequence of eqs. (7), (8), the brightness equation, eq. (6), now reads as

$$B = \alpha\, EQE_{LED}\, X. \tag{9}$$

According to Eq.(9), for a particular module with an unknown (but constant) EQE, and for a constant α (geometry factor G constant, internal and external conversion factors C_{int}, C_{ext} constant), the brightness B of every picture should be the same as long as the exposure X is constant. In other words, as long as X is constant, it is possible to choose any combination of J_e, t_s, A_s, and ISO to obtain the same brightness. Therefore also, instead of plotting graphs like those in **Figures 17 to 20** a plot of B in dependence of X should give a universal curve.

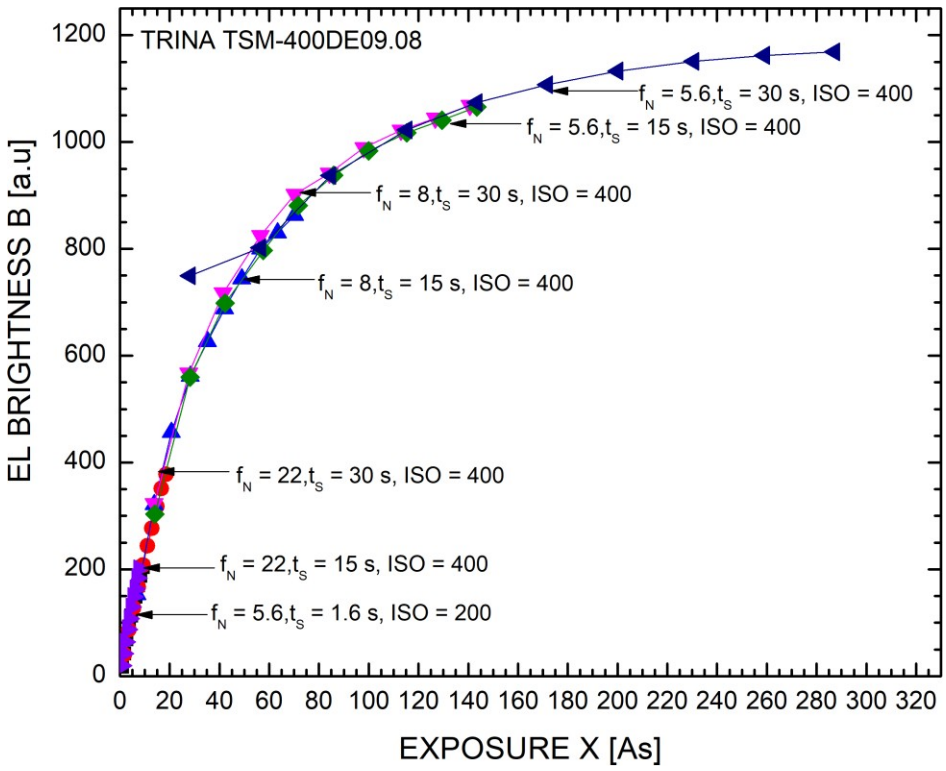

Figure 22: Universal Brightness Curve Depends Only on The Exposure X And Not on The Single Values of The Camera Settings.

Figure 22 shows the curves, which we get from **Figures. 17 to 20** by combining all measurement parameters for the Trina module. Indeed, all data fall on the same line. We observe the expected universal curve. This figure validates our camera model. In addition, however, it shows also that the saturation behavior of the brightness *B* is not due to a change of the recombination within the module: We obtain the same brightness with low as well as with high current (densities) as long as *X* is constant.

3.2.2.3 Saturation behavior

Similar to Figures. 17 to 20, for brightness values above B = 500, the brightness tends to saturate. Mathematically, we describe the saturation behavior by a charging equation via

$$B = B_\infty \ (1 - e^{-X/X_0}). \tag{10}$$

On one hand, for $X >> X_0$ the exponential function tends to zero and we get the saturation value

$$B = B_\infty . \tag{11}$$

On the other hand, for $X << X_0$, it is possible to approximate the exponential function of Eq.(10) by

$$e^{-X/X_0} = 1 - \frac{X}{X_0}. \tag{12}$$

Inserting Eq.(12) into Eq.(10) yields

$$B = \frac{B_\infty}{X_0} X. \tag{13}$$

Therefore, for small X, according to Eq. (12), we expect a linear dependence of B on X with the straight line going through zero. And, indeed, in this regime a linear behavior is also observed for the high efficiency module in **Figure 22**. Later, we will show that the linear behavior is even better observed for multicrystalline modules. Due to the low minority carrier lifetime, they emit only a small number of photons. Therefore, whatever the camera settings and the injected current is, the pixel sensors never get into saturation. In contrast, not only for the module of **Figure 22** but also for the other modules containing single crystalline, highly efficient cells, we are able to see the linear regime as well as the saturation behavior.

We explain the saturation dependence of B by the nonlinearity of the camera chip for high brightness: The pixel capacitors go into saturation. In our model, this is represented by the conversion factor $C_{int.}$ In the evaluation of chapter 6, we will only use the linear part of our measurements.

The experimental results gotten from the electroluminescence measurements of different silicon solar panels are studied in this thesis and we try to understand the differences based on the modules and also from our camera. Saturation of the sensor was more in the monocrystalline modules than in the multicrystalline modules.

Some of these differences can be attributed to the difference in the characteristics of the module such as their open circuit voltage and short circuit current. These were also some faults on the multicrystalline modules. The process of measuring the electroluminescence of all the modules was the same.

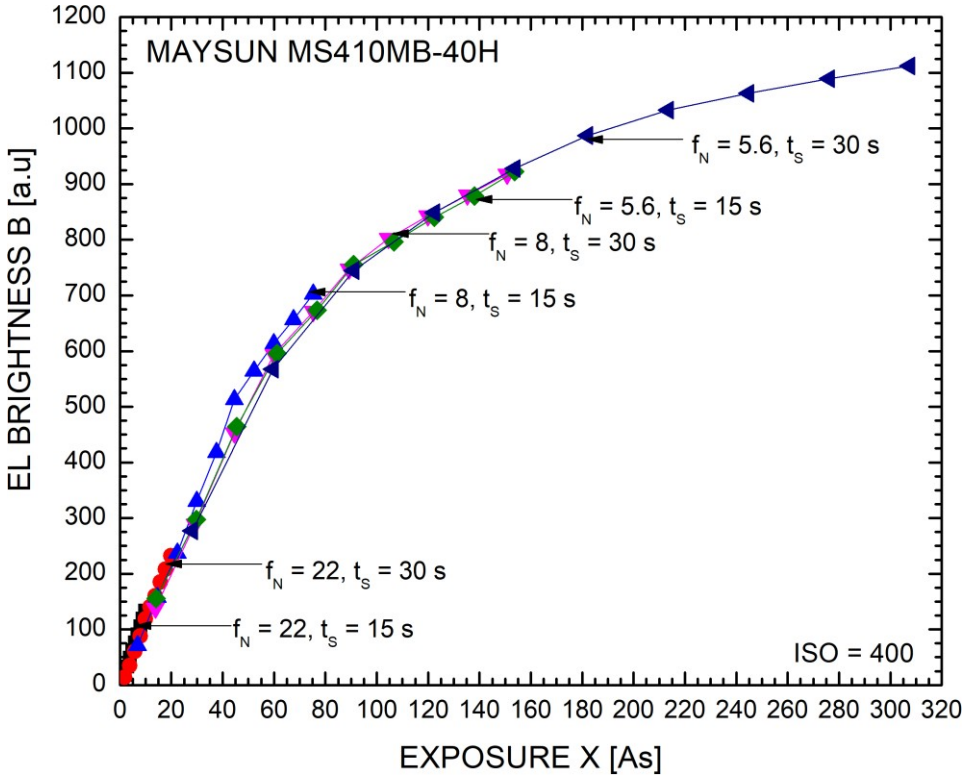

Figure 23: Changes In EL Brightness as Shutter Time and F-Number Changes in The Maysun Module.

Figures 22 to 27 shows the results of the electroluminescence measurements of the different modules at different camera settings. It is observed that the plots go linearly until values of electroluminescence brightness above 500, the camera goes into saturation.

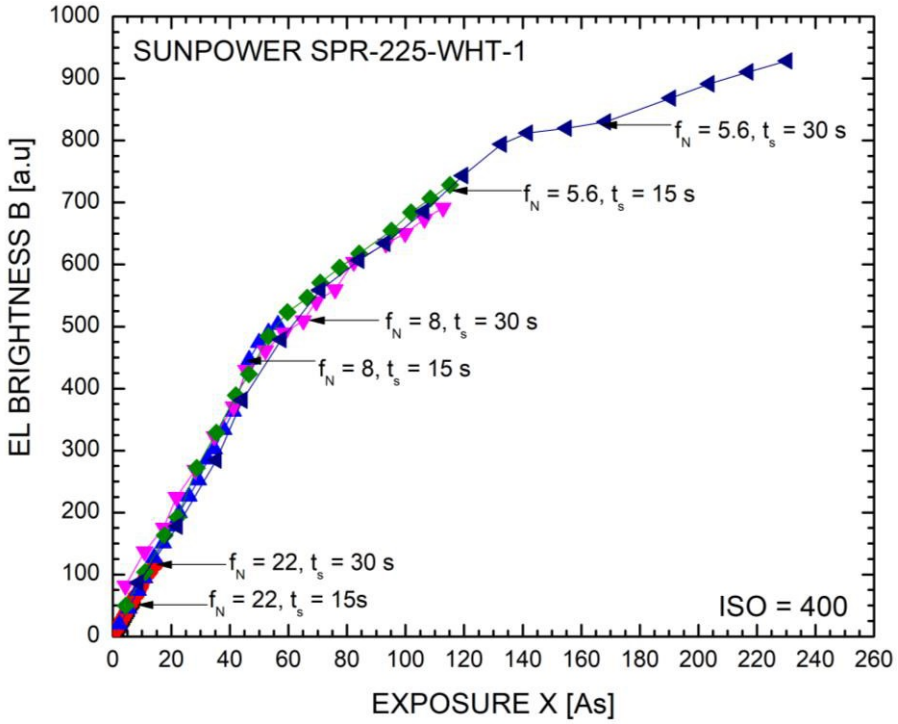

Figure 24: Changes In EL Brightness as Shutter Time and F-Number Changes in The Sun power module.

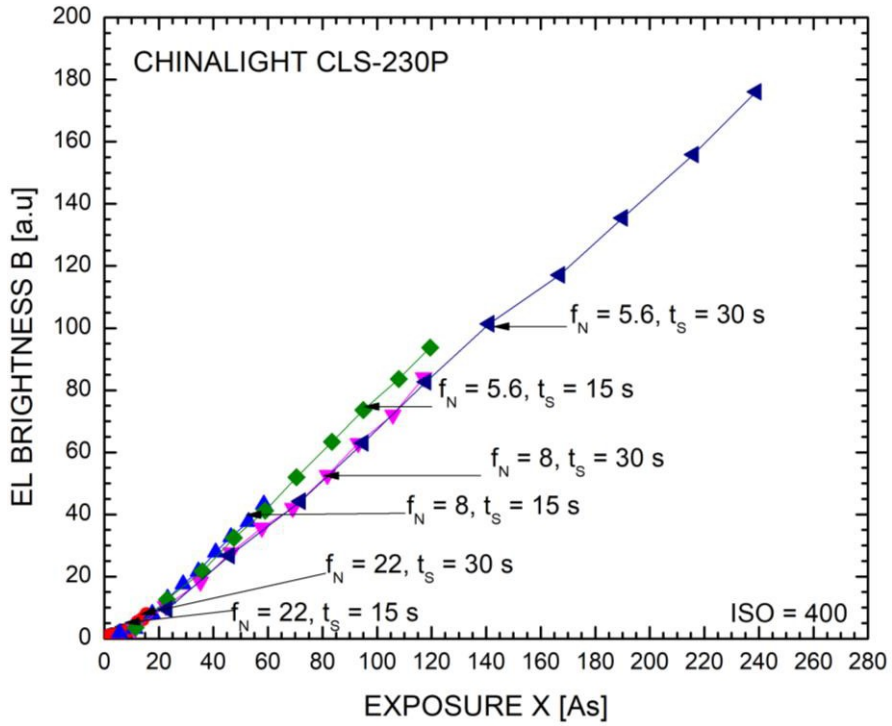

Figure 25: Changes In EL Brightness as Shutter Time and F-Number Changes In The Chinalight Module.

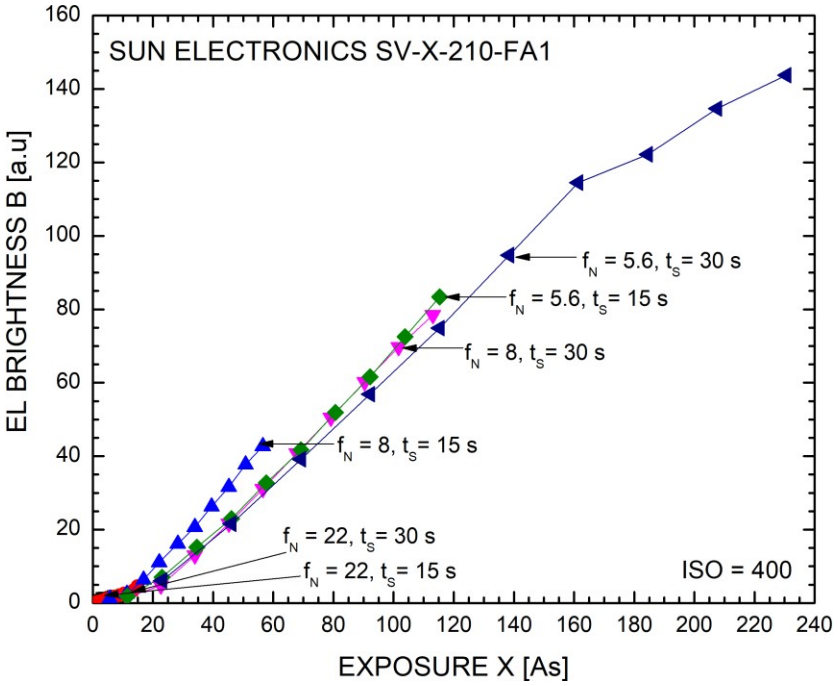

Figure 26: Changes In EL Brightness as Shutter Time and F-Number Changes in The Sun Electronics Module.

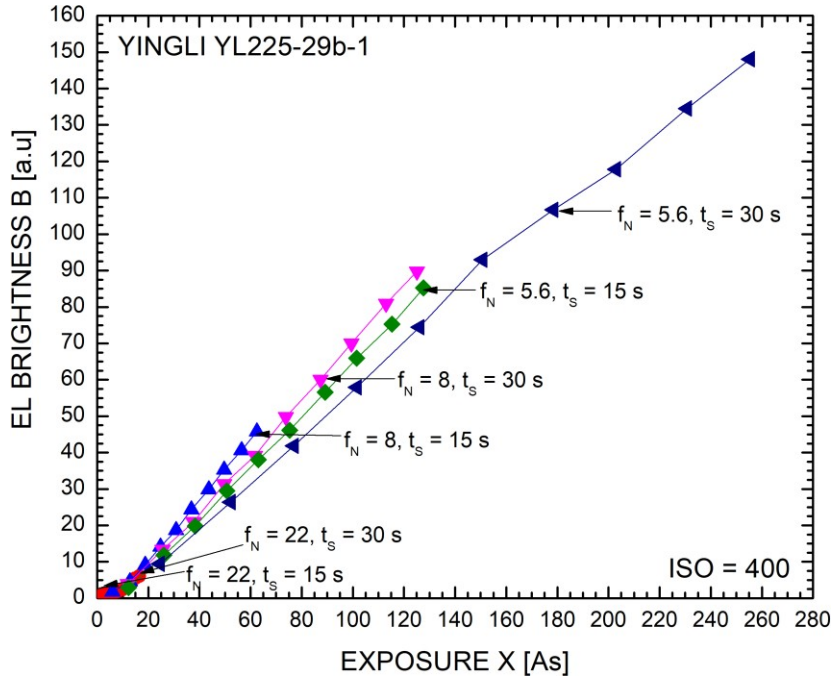

Figure 27: Changes In EL Brightness as Shutter Time and F-Number Changes in The Yingli Module.

Table 4: Detailed characteristics of module cells

Name of module	Total Number of cells	V_{oc} of module [V]	V_{oc} of cell [mV]	Number of cells in series	Number of cells in parallel	J_{sc} per cell [mA/cm^2]	I_{sc} of module [A]	Area of cell [cm^2]	Slope S_H [$A^{-1}s^{-1}$]	Cell Technology
Maysun MS410MB-40H	80	53.24	670	80	-	40	9.8	220.5	11	Halfcell heterojunction technology
Trina TSM-400DE09.08	120	41.4	690	60	2	42	12.28	147	21	Halfcell heterojunction technology
Sunpower SPR-225-WHT-1	72	48.5	660	72	-	38	5.87	156.25	10	Maxeon Si n-type
Sun electronics SV-X-210-FA1	114	23.1	600	38	3	33	12	120	0.75	String ribbon Sovello Si p-type
Chinalight CLS-230P	60	37.4	610	60	-	34	8.3	240.3	0.8	Block cast Si p-type
Yingli YL225-29b-1	60	36.5	600	60	-	36	8.2	225	0.7	Block cast Si p-type

Table 4 gives a detailed description of measured and calculated characteristics of the modules used in this thesis such characteristics include: the cell area, number of cells in parallel or series and these values vary in the different modules measured, even in modules of similar parameters.

From the electroluminescence images produced for each of the modules, some faults were noticed in some of the modules.

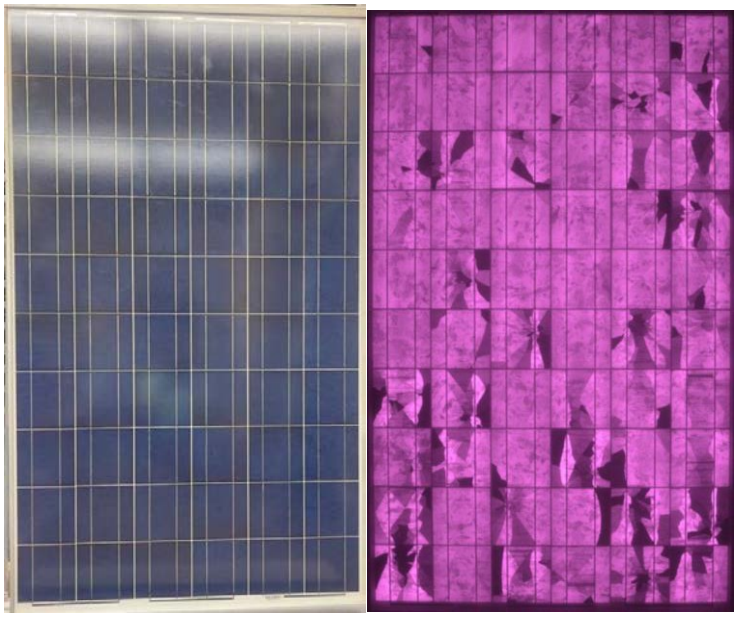

Figure 28: EL Image showing faults & normal image of Chinalight module.

Figure 28 shows the faults of a panel that are not easily seen with the eyes which is another advantage of the electroluminescence test. An IV measurement of the module was done and this fault was not indicated. These faults are another reason for some of the scatter in some of the module's electroluminescence plots.

Figure 29 shows the illuminated IV measurement of the chinalight module. It doesn't show any possible fault in the module but with the help of the electroluminescence image this can be seen.

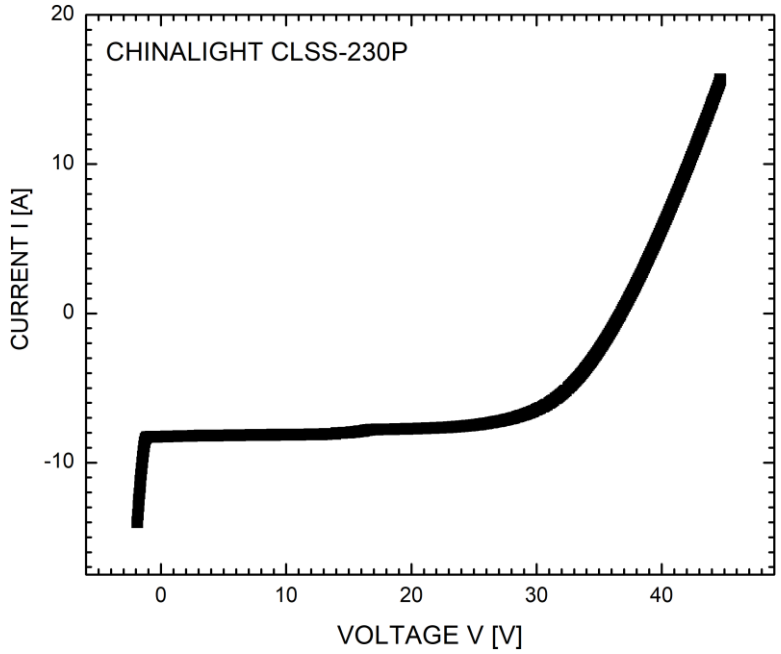

Figure 29: Normal IV Curve of The Chinalight Module Indicating No Faults.

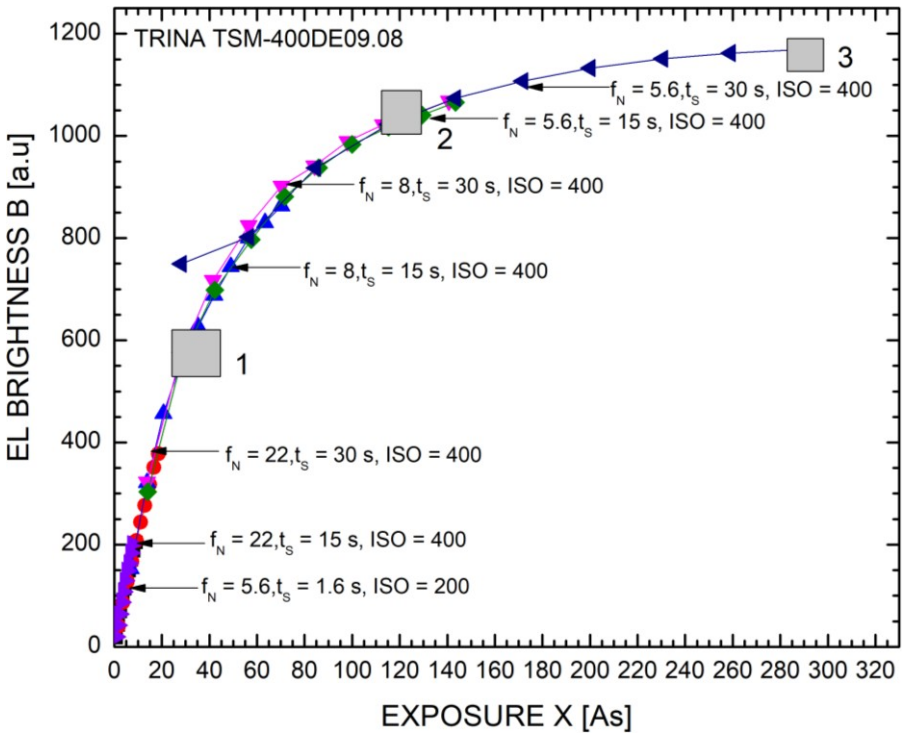

Figure 30: Trina Plot Showing Where the Histogram Images are Taken.

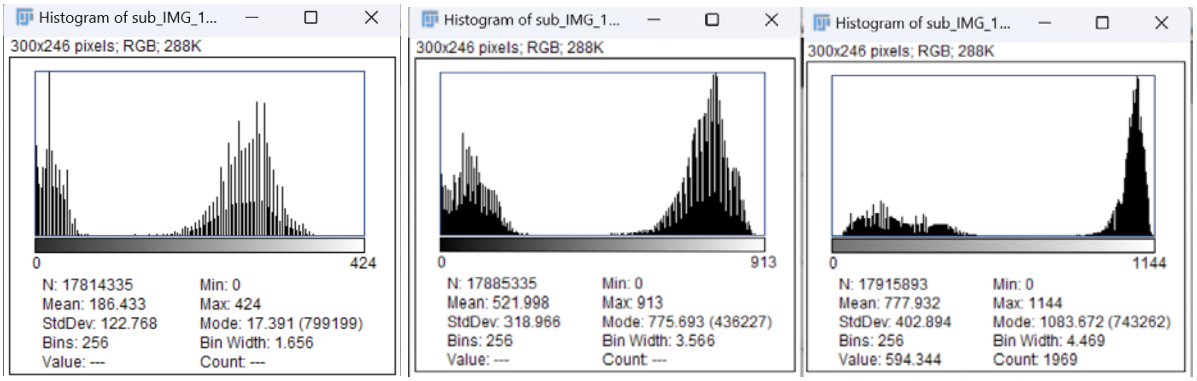

Figure 31: Histograms Showing The EL Brightness in Pixels at Different Measurements.

As can be seen from the images in **Figure 31** the histogram curve moves from the left to the right indicating that the more the current is increased the brighter the electroluminescence we get. The above histogram is for the Trina module (from figure 30). From the first image and the mid image are from 20% and 70% of the short circuit current at f-number = 5.6, shutter time = 15 seconds and ISO = 400, the final image is that of f-number = 5.6, ISO = 400, but the shutter time is at 30 seconds and at 100% of the short circuit current. These histograms are a combination of the red blue and green channels. It easy to see when the sensor goes into saturation. As can be seen below. The graph is from 0 to 1144, this is because all channels are viewed together each pocket having 288 possibilities. Once the peak gets steeper you can see the corresponding saturation in **Figure 30**.

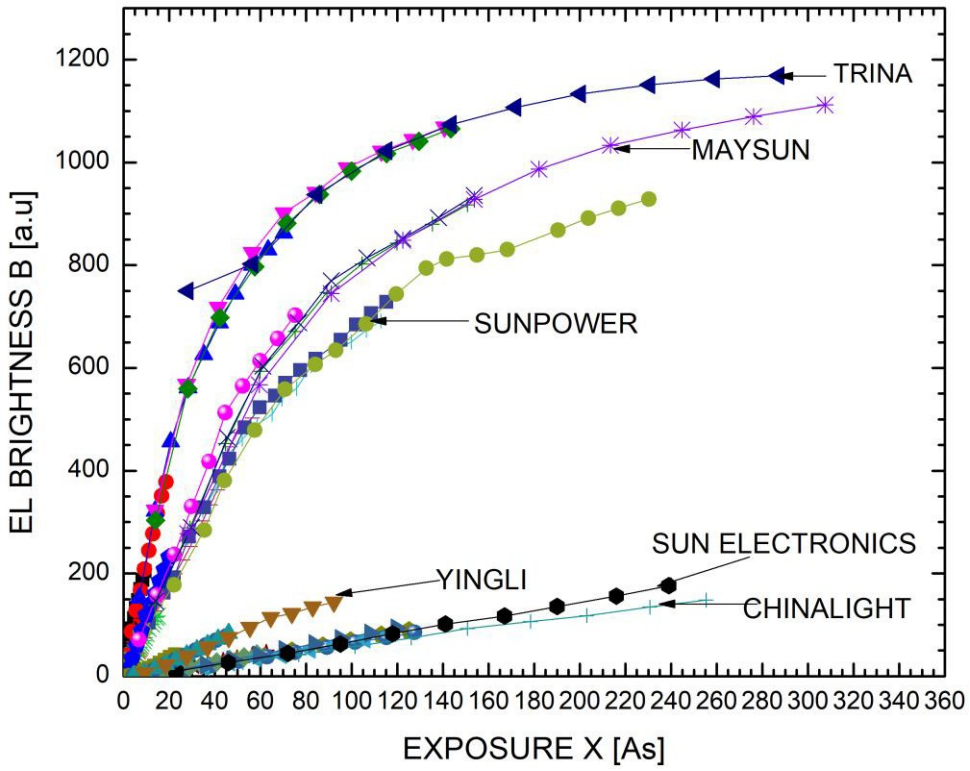

Figure 32: To View the Difference In Electroluminescence Between Monocrystalline And Multi-crystalline Modules.

Figure 32 the first three modules (Trina, May sun and Sun power) are single crystalline silicon modules they emit brighter luminescence as compared to the lower three (Yingli, Sun Electronics and Chinalight) which are multi-crystalline silicon modules. For all modules the shutter duration and f-number combination were varied and ISO kept constant to produce different images and measure the changes of the electroluminescence. They modules were measured from 10% to 100% of their short circuit current. Each of these modules have their specific characteristics as expressed in **table 4** their different characteristics contribute to their different electroluminescence.

3.3 Reciprocity Theorem, An Experimental Test

3.3.1 Reciprocity theorem

In this thesis silicon solar cells were the only type of solar cells used, this is because with efficiencies η up to η = 26.7%*(Green & Ho-Baillie, 2019)* silicon solar cells reach high efficiencies. Nevertheless, light emission from silicon is quite inefficient, with an external luminescence quantum efficiency $EQE_{LED} \approx 1\%$ for the very best solar cells.

The external luminescence quantum efficiency EQE_{LED} is related to the open circuit voltage V_{oc} of a solar cell via *(Kirchartz & Rau, 2008).*

$$\Delta V_{OC} = V_{OC} - V_{OC}{}^{rad} = kT/q \quad \ln EQE_{LED} \tag{13}$$

Here, ΔV_{oc} is the difference between the actual open circuit voltage V*oc* of the real cell and V_{oc}^{rad} is the theoretical, uppermost efficiency if all carriers recombined radiatively. If the cell had reached $V_{oc}{}^{rad}$, the EQE_{LED}would be $EQE_{LED} = 1 = 100\%$. If we introduce the log to the base of 10 instead the natural log, i.e. ln, in Eq.(13), we obtain

$$\Delta V_{OC} = \frac{kT}{q} \ln(10) \log EQE_{LED} \tag{14}$$

$$= 2.30 \frac{kT}{q} \log EQE_{LED},$$

Rewriting Eq.(13) yields

$$V_{OC} = V_{OC}{}^{rad} + 2.30\ kT/q \quad \log EQE_{LED},$$

and the derivative is

$$\frac{dV_{oc}}{d \log EQE_{LED}} = 2.30 \text{ kT/q} \tag{15}$$

The meaning of Eq.(15) is simple: For every increase of EQE_{LED} by a factor of ten (then the log changes by one unit), the open circuit voltage increases by a value of 2.3 kT/q, which at room temperature is an increase of 60 mV. A cell with an $EQE_{LED} \approx 1$ % has an open circuit voltage which ranges 120 mV below its maximum possible open circuit voltage, which it had, when there was only radiative recombination.

It is important to know that the maximum possible open circuit voltage $V_{oc}{}^{rad}$ for solar cells is different from cell to cell. In particular, it depends on the light trapping, i.e. on the path elongation of the infrared radiation in the cell *(Kirchartz & Rau, 2008).*

3.3.2 Experimental analysis

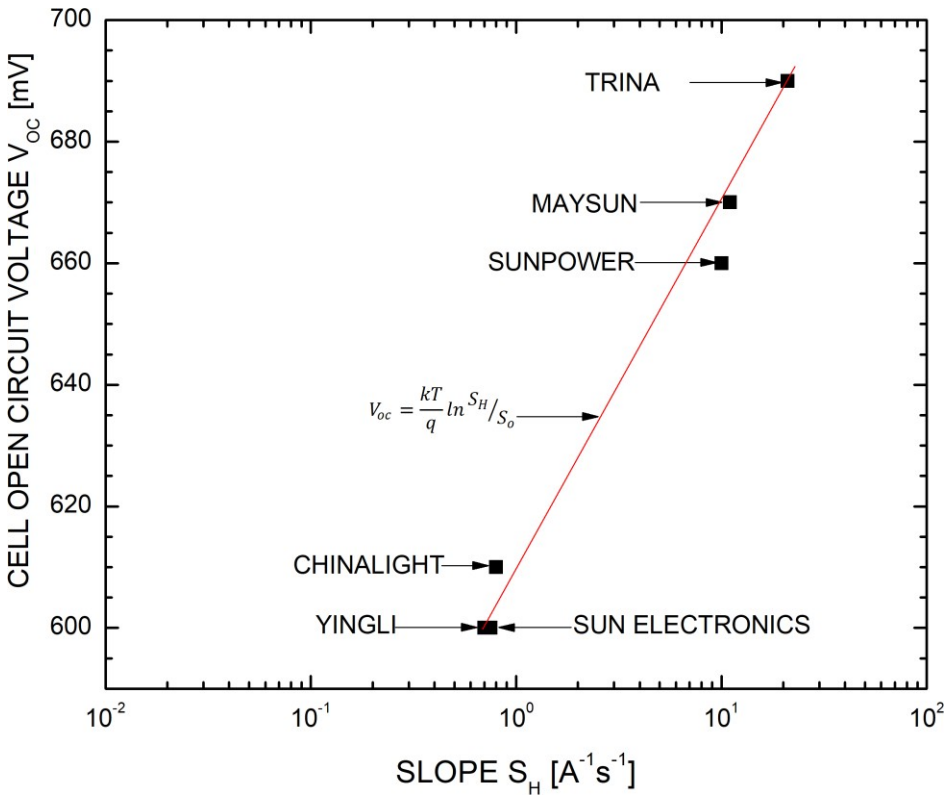

Figure 33: The open circuit voltage follows the log of S_H. The red line is the best fit to the experimental data with a slope of 2.30 $kT/q \approx 60$ mV at room temperature.

Figure 33 shows the open circuit voltages V_{oc} of an *average* cell in our modules. In reality, we were not able to measure the open circuit voltage at just the cell from which we took the electroluminescence picture. However, we deduced the cell's open circuit voltage by measuring the open circuit voltage of the module and dividing it by the number of series connected cells. Therefore, we estimate the error bar for the cells' open circuit voltage to be about +/- 5 mV.

The x-axis in **Figure 33** stems from the slope of the measurements of the brightness B of the modules in dependence on the exposure X, such as in **Figure 27**. We define the "brightness slope" as

$$S_H = \frac{dB}{dX} \tag{16}$$

Figure 33 shows that the open circuit voltage is higher, when the brightness slope S_H is higher. This is easy to understand on the basis of our Eq.(6). According to our camera model, the brightness B is written as

$$B = \alpha\, X\, EQE_{LED}. \tag{17}$$

Consequently, it holds

$$S_H = \frac{dB}{dX} = \alpha\, EQE_{LED}, \tag{18}$$

and

$$\log S_H = \log \alpha + \log EQE_{LED}. \tag{19}$$

We are interested in the slope of Figure 33, which is

$$\frac{dV_{oc}}{d \log S_H} \equiv \frac{dV_{oc}}{d\, EQE_{LED}} = 2.30 kT/q. \tag{20}$$

According to Eq.(20), for the cells in the different modules we would expect in Figure 33 that all voltages are on one line with a slope of 2.30 kT/q, this means with an increase of 60 mV per decade increase of S_H. However, this clearly holds under the condition that all cells in all of our modules have the same maximum possible radiative efficiency limit V_{oc}^{rad}. This is not exactly true: The new high efficiency cells in the monocrystalline modules are expected to have a higher limit than the older multi-crystalline cells, simply because of better light trapping. Nevertheless, we will show in the following that this approximation yields a good fit to all or our data.

Figure 33 shows a straight line with a slope of 60 mV/decade which is the best fit to our data for the high efficiency modules containing crystalline silicon cell. To push our evaluation to the limit, we use this line to convert the S_H-axis into an absolute axis for the luminescence quantum efficiency EQE_{LED}. For that purpose, we use a simple idea: If we knew the absolute value of EQE_{LED} of the cells within at least one module, we could calculate the so far unknown parameter α in our eq.(18). Then, again via Eq. (18), we would be able to convert *all* S_H-values of all modules into absolute values for the quantum efficiency EQE_{LED}.

The line in **Figure 33** goes exactly though the data point for the Trina module and follows the equation

(21)

$$V_{oc} = 2.30 \frac{kT}{q} \log S_H + V_o = \frac{kT}{q} \ln S_H + V_0,$$

with V_0 = 608 mV. Therefore, for $S_H = 1$ it holds $V_{oc} = V_0$. Writing

$$V_0 = -2.30 \frac{kT}{q} \log S_0 \tag{22}$$

yields

$$V_{oc} = 2.30 \frac{kT}{q} \log S_H / S_o \tag{23}$$

or

$$V_{oc} = \frac{kT}{q} \ln S_H / S_o \tag{24}$$

with $S_0 = 6.31 \times 10^{-11}$ $(As)^{-1}$.

Unfortunately, we were not able to measure absolute values the quantum efficiency EQE_{LED} of our modules. Therefore, we use the following trick to calculate the value of α: The world-wide best silicon cell with an EQE_{LED} = 1.6 % has an open circuit voltage of V_{oc} = 740 mV, (which corresponds to a V_{oc}^{rad} = *847* mV for an EQE_{LED} = 1). Therefore, we extrapolate the line of **Figure 33** to 740 mV and assume this world best cell would also be on our fitting line.

Then, by inserting Eq.(19) for this world record cell into eq.(21) yields

$$V_{oc} = kT/q(\ln \alpha + lnEQE_{LED}) + V_0. \tag{22}$$

With the known values of V_{oc} = 740 mV, V_o = 608 mV, and EQE_{LED} = 1.6 %, we obtain $\alpha \approx 1 \times 10^4$ $A^{-1}s^{-1}$. As a consequence of knowing this α-value, Table 5 and **Figure 34** are now able to give approximate EQE_{LED} – values for all of our modules via

$$EQE_{LED} = S_H/\alpha. \tag{23}$$

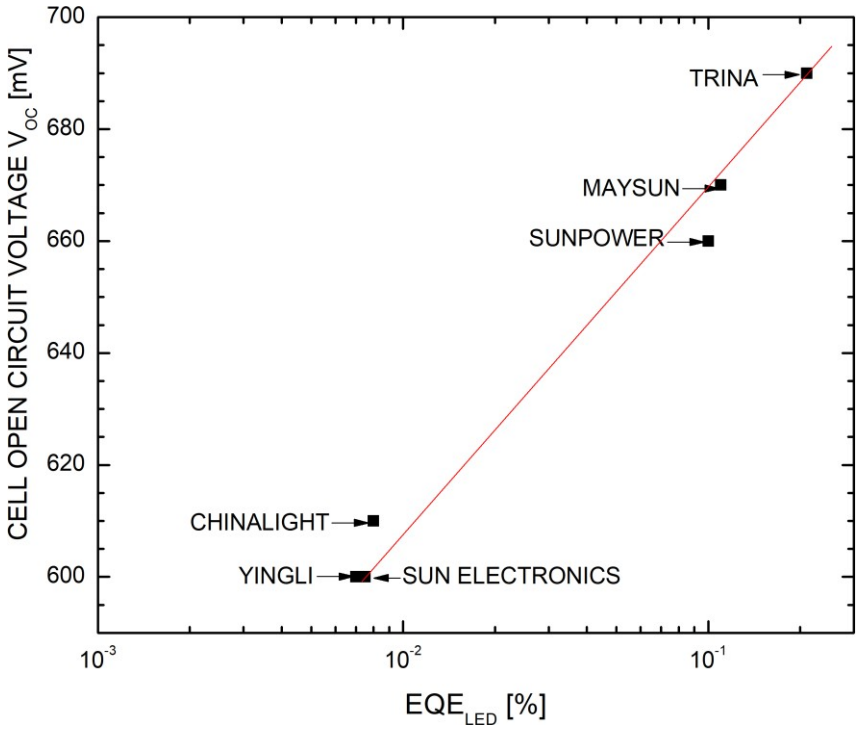

Figure 34: External radiative quantum efficiencies of the measured solar modules. The open circuit voltage depends logarithmically on the EQE_{LED}. We assumed that all cells in the modules have the same radiative limit of the open circuit voltage. The red curve fits the data well.

Table 5: Brightness slope values and calculated radiative quantum efficiencies of our modules.

NAME OF MODULES	**SLOPE S_H [$A^{-1}s^{-1}$]**	**OPEN CIRCUIT VOLTAGE V_{OC} [V]**	**EQE_{LED} [%]**
Trina	21 ± 1	690	0.21
Maysun	11 ± 1	670	0.11
Sunpower	10 ± 1	660	0.1
Sun electronics	0.75 ± 0.05	600	0.0075
Chinalight	0.8 ± 0.05	610	0.008
Yingli	0.7 ± 0.1	600	0.007

Figure 34 proves our predicted outcome and also the reciprocity theorem. Table 5 gives the list of the values plotted and also the degree of possible errors as the process required extrapolation.

CONCLUSION

In this work it was experimented and demonstrated how one can use a normal camera to carry out electroluminescence test and how the camera setting play a large role in the electroluminescence results obtained. The project also proved that with the commercial camera electroluminescence images one can also detect faults from a panel. This was with the Chinalight module that with a current-voltage measurement of the panel some defects are not noticed from the output of the I-V curve.

It is evident that with a commercial camera one can make electroluminescence measurement but this thesis also explained how the sensitivity of the sensor should be taken into consideration when selecting the camera to use for electroluminescence tests, and how the different parameters in photography have an effect on the outcome and on dark electroluminescence. From the results obtained, the best setting with a canon EOS 4000D for electroluminescence measurement would be at F-number $f_N = 8$, ISO = 400 and the shutter time $t_S = 15$ s.

This research also gave an experimental prove to the Rau's reciprocity theorem that the open circuit voltage of a module changes by an output of 60mV per decade of the electroluminescence quantum efficiency. This experiment also gives the opportunity that academic laboratories can make use of commercial cameras to perform electroluminescence test and reduce the cost as the camera are more affordable.

An electroluminescence image provides so much information about a photovoltaic module and there is more to be understood when using a commercial camera to perform this task.

REFERENCES

2012 Defect detection in Modules with EL. (n.d.).

Africa has the world's most potential for solar energy | World Economic Forum. (n.d.). Retrieved July 29, 2023, from https://www.weforum.org/agenda/2022/09/africa-solar-power-potential/

Ahanogbe, K. F., Alvarez, J., Jaffré, A., Connolly, J. P., Gueunier-Farret, M. E., Fourmond, E., El-Whibi, S., Fave, A., Carroy, P., Djebbour, Z., & Kleider, J. P. (2022). Electroluminescence analysis of silicon interdigitated back contact solar cells with a front surface selective band offset barrier. *EPJ Photovoltaics*, *13*, 16. https://doi.org/10.1051/EPJPV/2022015

Baghel, N. S., & Chander, N. (2022). Performance comparison of mono and polycrystalline silicon solar photovoltaic modules under tropical wet and dry climatic conditions in east-central India. *Clean Energy*, *6*(1), 929–941. https://doi.org/10.1093/ce/zkac001

Ballif, C., Haug, F. J., Boccard, M., Verlinden, P. J., & Hahn, G. (2022). Status and perspectives of crystalline silicon photovoltaics in research and industry. In *Nature Reviews Materials* (Vol. 7, Issue 8, pp. 597–616). Nature Research. https://doi.org/10.1038/s41578-022-00423-2

Bedrich, K. G., Bliss, M., Betts, T. R., & Gottschalg, R. (n.d.). *Electroluminescence Imaging of PV Devices: Camera Calibration and Image Correction*.

Bliss, M., Wu, X., Bedrich, K. G., Bowers, J. W., Betts, T. R., & Gottschalg, R. (2015). Spatially and spectrally resolved electroluminescence measurement system for photovoltaic characterisation. *IET Renewable Power Generation*, *9*(5), 446–452. https://doi.org/10.1049/iet-rpg.2014.0366

Brown, T. (2010). Construct validity: A unitary concept for occupational therapy assessment and measurement. In *Hong Kong Journal of Occupational Therapy* (Vol. 20, Issue 1, pp. 30–42). https://doi.org/10.1016/S1569-1861(10)70056-5

Chen, H., Zhao, H., Han, D., & Liu, K. (2019). Accurate and robust crack detection using steerable evidence filtering in electroluminescence images of solar cells. *Optics and Lasers in Engineering*, *118*, 22–33. https://doi.org/10.1016/j.optlaseng.2019.01.016

Ciocia, A., Carullo, A., DI Leo, P., Malgaroli, G., & Spertino, F. (2019). Realization and Use of an IR Camera for Laboratory and On-field Electroluminescence Inspections of Silicon Photovoltaic Modules. *Conference Record of the IEEE Photovoltaic Specialists Conference*, 2734–2739. https://doi.org/10.1109/PVSC40753.2019.8980711

Colvin, D. J., Schneller, E. J., & Davis, K. O. (2022). Cell dark current–voltage from non-calibrated module electroluminescence image analysis. *Solar Energy*, *244*, 448–456. https://doi.org/10.1016/J.SOLENER.2022.08.043

Colvin, D. J., Schneller, E. J., Horner, G. S., Gabor, A. M., & Davis, K. O. (2021). Evaluating Impact on Electroluminescence Image Quality and Quantitative Analysis

using Different Camera Technologies. *Conference Record of the IEEE Photovoltaic Specialists Conference*, 1057–1061. https://doi.org/10.1109/PVSC43889.2021.9518826

Cordero, E. F., Ploss, B., & Sivakov, V. (2016). *Hydrogen Generation on Silicon Nanostructures*.

Dioha, M. O., & Kumar, A. (2020). Exploring the energy system impacts of Nigeria's Nationally Determined Contributions and low-carbon transition to mid-century. *Energy Policy*, *144*. https://doi.org/10.1016/j.enpol.2020.111703

Drabczyk, K., Kulesza-Matlak, G., Drygała, A., Szindler, M., & Lipiński, M. (2016). Electroluminescence imaging for determining the influence of metallization parameters for solar cell metal contacts. *Solar Energy*, *126*, 14–21. https://doi.org/10.1016/j.solener.2015.12.029

Frazão, M., Silva, J. A., Lobato, K., & Serra, J. M. (2017). Electroluminescence of silicon solar cells using a consumer grade digital camera. *Measurement: Journal of the International Measurement Confederation*, *99*, 7–12. https://doi.org/10.1016/J.MEASUREMENT.2016.12.017

Fuyuki, T., & Kitiyanan, A. (2009). Photographic diagnosis of crystalline silicon solar cells utilizing electroluminescence. *Applied Physics A: Materials Science and Processing*, *96*(1), 189–196. https://doi.org/10.1007/s00339-008-4986-0

Green, M. A., & Ho-Baillie, A. W. Y. (2019). Pushing to the Limit: Radiative Efficiencies of Recent Mainstream and Emerging Solar Cells. In *ACS Energy Letters* (Vol. 4, Issue 7, pp. 1639–1644). American Chemical Society. https://doi.org/10.1021/acsenergylett.9b01128

Henisch, H. K., Dennis, J., & Hanoka, J. I. (1965). CRYSTAL GROWTH IN GELS. In *J. Phys. Chem. Solids Pergamon Press* (Vol. 26).

Home | Delta Elektronika. (n.d.). Retrieved July 31, 2023, from https://www.delta-elektronika.nl/

IR-Photo.net | Infrared Photography. (n.d.). Retrieved July 31, 2023, from http://www.ir-photo.net/ir_imaging.html

Jain, U. (2016). *Characterization of CMOS Image Sensor*.

Kelby, Scott. (2013). *The Adobe Photoshop CS6 book for digital photographers*. 453.

Kirchartz, T., & Rau, U. (2008). Detailed balance and reciprocity in solar cells. *Physica Status Solidi (A) Applications and Materials Science*, *205*(12), 2737–2751. https://doi.org/10.1002/pssa.200880458

Lulé, T., Benthien, S., Keller, H., Mütze, F., Rieve, P., Seibel, K., Sommer, M., & Böhm, M. (2000). Sensitivity of CMOS Based Imagers and Scaling Perspectives. In *IEEE TRANSACTIONS ON ELECTRON DEVICES* (Vol. 47, Issue 11).

Mccleland, J. C., Kwembur, I., Dix-Peek, R., Vorster, F., & Van Dyk, E. (n.d.). *IMPLEMENTATION OF TECHNICAL SPECIFICATIONS TO STANDARDISE AND IMPROVE ELECTROLUMINESCENCE IMAGING TEST SETUPS*.

MIX-DEN: ELECTROLUMINESCENCE AND DIODE LASERS. (n.d.).

Monocrystalline vs. Polycrystalline Solar Panels (2023 Guide). (n.d.). Retrieved July 29, 2023, from https://www.thisoldhouse.com/solar-alternative-energy/reviews/monocrystalline-vs-polycrystalline-solar-panels

Numerical study of a steam methane reformer integrated membrane system for 250 kg/day hydrogen production. (2022). https://www.researchgate.net/publication/370068488

Photovoltaics and electricity - U.S. Energy Information Administration (EIA). (n.d.). Retrieved July 29, 2023, from https://www.eia.gov/energyexplained/solar/photovoltaics-and-electricity.php

Rau, U. (2007). Reciprocity relation between photovoltaic quantum efficiency and electroluminescent emission of solar cells. *Physical Review B - Condensed Matter and Materials Physics*, *76*(8). https://doi.org/10.1103/PhysRevB.76.085303

Schneider, C. A., Rasband, W. S., & Eliceiri, K. W. (2012). NIH Image to ImageJ: 25 years of image analysis. *Nature Methods 2012 9:7*, *9*(7), 671–675. https://doi.org/10.1038/nmeth.2089

Sulas, D. B., Johnston, S., & Jordan, D. C. (2019). Comparison of photovoltaic module luminescence imaging techniques: Assessing the influence of lateral currents in high-efficiency device structures. *Solar Energy Materials and Solar Cells*, *192*, 81–87. https://doi.org/10.1016/j.solmat.2018.12.022

Swanson, R. M. (2006). A vision for crystalline silicon photovoltaics. In *Progress in Photovoltaics: Research and Applications* (Vol. 14, Issue 5, pp. 443–453). https://doi.org/10.1002/pip.709

Which Aperture is Best for Portraits or Landscape (n.d.). Retrieved July 31, 2023, from https://mastinlabs.com/blogs/photoism/which-aperture-is-best

Xu, B., Mou, K., Institute of Electrical and Electronics Engineers. Harbin Section, & Institute of Electrical and Electronics Engineers. (n.d.). *Proceedings of 2020 IEEE 5th Information Technology and Mechatronics Engineering Conference (ITOEC 2020) : June 12-14, 2020, Chongqing, China*.

Ye, Y., Ye, Z., Gharghi, M., Zhu, H., Zhao, M., Wang, Y., Yin, X., & Zhang, X. (2014). Exciton-dominant electroluminescence from a diode of monolayer MoS 2. *Applied Physics Letters*, *104*(19). https://doi.org/10.1063/1.4875959

Yoshikawa, K., Kawasaki, H., Yoshida, W., Irie, T., Konishi, K., Nakano, K., Uto, T., Adachi, D., Kanematsu, M., Uzu, H., & Yamamoto, K. (2017). Silicon heterojunction solar cell with interdigitated back contacts for a photoconversion efficiency over 26%. *Nature Energy*, *2*(5). https://doi.org/10.1038/nenergy.2017.32

Zhang, Y., Wang, R., Wang, F., Zhu, D., Gong, X., & Cheng, X. (2023). Electroluminescence as a Tool to Study the Polarization Characteristics and Generation Mechanism in Silicon PV Panels. *Applied Sciences (Switzerland)*, *13*(3). https://doi.org/10.3390/app13031591

APPENDIX

Cells measured in each of the modules.

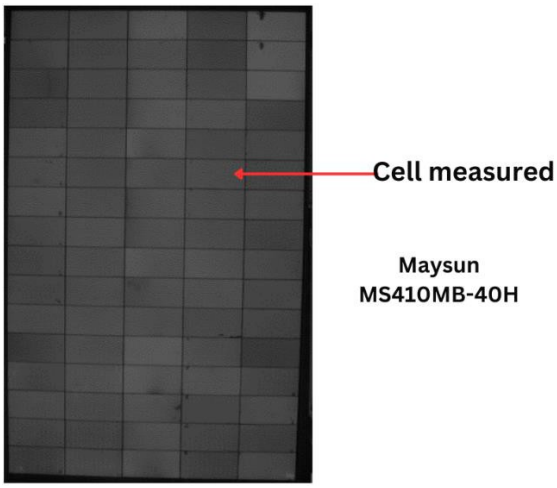

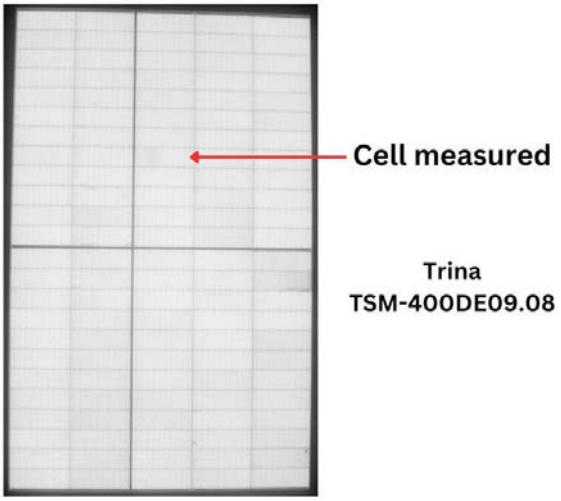

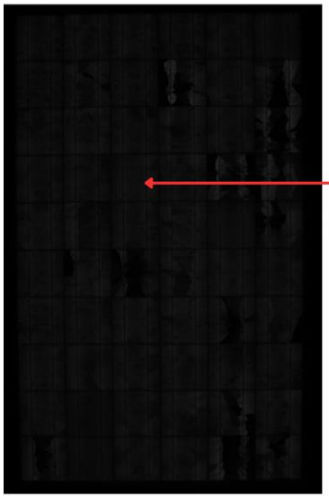

Yingli YL225-29b-1

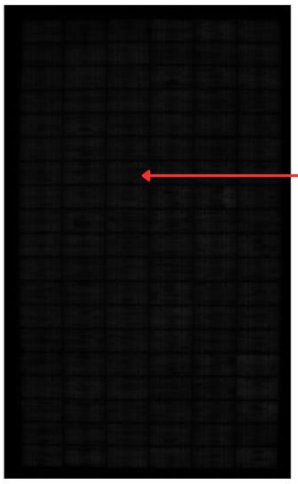

Sun electronics
SV-X-210-FA1

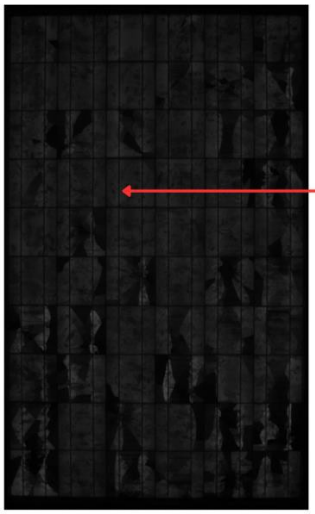

Chinalight
CLS-230P

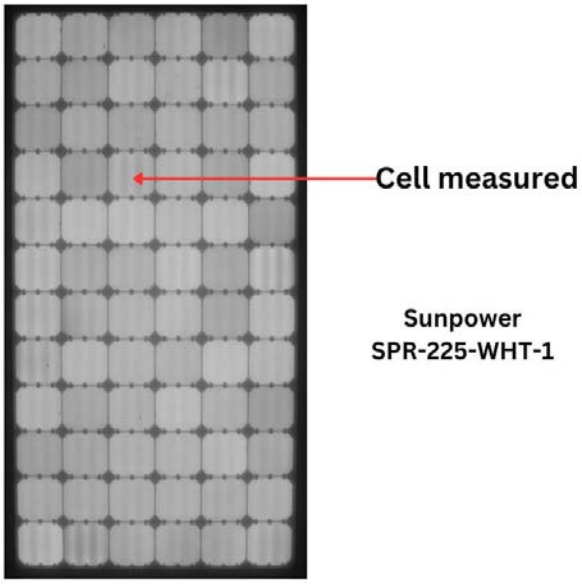
Cell measured
Sunpower
SPR-225-WHT-1